Department of Forest Products Technology

Development of a novel process for the production of man-made cellulosic fibers from ionic liquid solution

Anne Michud

Aalto University

DOCTORAL DISSERTATIONS

Aalto University publication series
DOCTORAL DISSERTATIONS 90/2016

Development of a novel process for the production of man-made cellulosic fibers from ionic liquid solution

Anne Michud

A doctoral dissertation completed for the degree of Doctor of Science (Technology) to be defended, with the permission of the Aalto University School of Chemical Technology, at a public examination held at the lecture hall Ke2 at the Department of Biotechnology and Chemical Technology on 10 June 2016 at 12.

Aalto University
School of Chemical Technology
Department of Forest Products Technology
Biorefineries

Supervising professor
Professor Herbert Sixta, Aalto University

Thesis advisor
Dr. Michael Hummel, Aalto University

Preliminary examiners
Professor Henri Chanzy, CNRS-CERMAV, France
Dr. Frank Hermanutz, ITCF, Germany

Opponent
Professor Hans-Peter Fink, Fraunhofer-Institute for Applied Polymer Research, Germany

Aalto University publication series
DOCTORAL DISSERTATIONS 90/2016

ISBN 978-952-60-6804-6 (printed)
ISBN 978-952-60-6805-3 (pdf)
ISSN-L 1799-4934
ISSN 1799-4934 (printed)
ISSN 1799-4942 (pdf)
http://urn.fi/URN:ISBN:978-952-60-6805-3

Unigrafia Oy
Helsinki 2016

Finland

441 697
Printed matter

Author
Anne Michud

Name of the doctoral dissertation
Development of a novel process for the production of man-made cellulosic fibers from ionic liquid solution

Publisher School of Chemical Technology

Unit Department of Forest Products Technology

Series Aalto University publication series DOCTORAL DISSERTATIONS 90/2016

Field of research Biorefineries

Manuscript submitted 17 February 2016 **Date of the defence** 10 June 2016

Permission to publish granted (date) 31 March 2016 **Language** English

☐ **Monograph** ☒ **Article dissertation** ☐ **Essay dissertation**

Abstract

This study presents the development of a novel process for producing man-made cellulosic fibers from an ionic liquid solution, the so called Ioncell-F process. It examines the full production chain from efficient dissolution of cellulose in ionic liquid to the suitability of the spun fibers for textile applications. A dry-jet wet spinning process consisting of the extrusion of a polymer solution at mild temperature through a multi-filament spinneret into an aqueous coagulation bath via an air gap was employed for the regeneration of cellulose into filaments. For preparation of the spinning dopes, 1-ethyl-3-methylimidazolium acetate and 1,5-diazabicyclo[4.3.0]non-5-enium acetate were used as solvents for different commercial dissolving pulps.

Both ionic liquids showed an excellent capability in dissolving cellulose at mild conditions. Minor cellulose depolymerization was obtained at a temperature below 85 °C with a low shearing rate. The intrinsic properties of the dissolved raw material, such as the degree of polymerization and molar mass distribution, exhibited a significant influence on the viscoelastic properties of the resulting polymer solution, and were monitored by oscillatory shear rheology and extensional rheology. The viscoelastic properties of the cellulose/ionic solution played a key role in determining the so called "spinning window" required to achieve optimal spinnability.

The tested 1-ethyl-3-methylimidazolium acetate/cellulose solution showed poor processing ability, while the 1,5-diazabicyclo[4.3.0]non-5-enium acetate/cellulose solution revealed effective spinning capability, resulting in the production of high-tenacity cellulosic staple fibers.

The fundamental spinning concepts were investigated and contributed to the determination of the spinning window. Cellulosic fibers, covering a wide spectrum of structural and mechanical properties, were manufactured by varying the applied stretch of the extruded filaments.

Ioncell fibers belong to the category of Lyocell fibers, provided that they are produced commercially, and display appropriate structural and mechanical behavior to be converted into yarn, and subsequently converted to knitted and woven fabrics. The excellent performance of the Ioncell spun yarn during the knitting and weaving process confirmed the competitive quality of the yarn and its suitability for the production of apparel. The future of this technology as an alternative to the viscose and NMMO-based Lyocell processes is promising, based on the development of a viable solvent-recovery step.

Keywords cellulose, ionic liquid, dry-jet wet spinning, man-made cellulosic fibers

ISBN (printed) 978-952-60-6804-6 **ISBN (pdf)** 978-952-60-6805-3

ISSN-L 1799-4934 **ISSN (printed)** 1799-4934 **ISSN (pdf)** 1799-4942

Location of publisher Helsinki **Location of printing** Helsinki **Year** 2016

Pages 137 **urn** http://urn.fi/URN:ISBN:978-952-60-6805-3

Preface

This doctoral dissertation was carried out at the Department of Forest Products Technology - School of Chemical Technology, Aalto University from 2011 to 2016 under the supervision of Prof. Herbert Sixta. This study started within the FuBio (Future Biorefinery) Products from Dissolved Cellulose programme financed by TEKES (Finnish Funding Agency for Innovation) and FIBIC (Finnish Bioeconomy Cluster) and continued within the ACel (Advanced Cellulose to Novel Products) programme of CLIC innovation (former FIBIC). I would also like to acknowledge the Paper Engineers' Association and the Walter Ahlström and Runar Backström Foundations for their additional financial support during this thesis.

First, I would like to express my deepest gratitude to my supervisor Prof. Herbert Sixta for offering me the possibility to participate in this extremely challenging project. Thank you for giving me your trust not only once but twice! Being part of this research gave a different turn to my life, both in professional and personal aspects. Your continuous guidance and questioning pushed my everyday efficiency to a maximum. From now on, your “I don't understand Anne, why isn't it possible?” will follow me every where I go.

My second deepest gratitude goes to Dr. Michael Hummel who has been my mentor since the very beginning of my work as part of the ionic liquid team, which is nowadays commonly called the spinning team. Your daily advice, help and encouragement in basically EVERYTHING was more than precious. I could not have wished for a better advisor, this work could not have been so successful without your continuous support. I will always remember your “Anne, this is very good but you need to write it all again” or how you made fun of my way of pronouncing the words “pulp” or “bus”. Thank you for being an amazing advisor, office-mate and friend (... and chocolate supplier).

I would like to thank all the members of the Biorefineries research group for creating such a friendly and pleasant working environment. The many coffee breaks, after work beers and group dinners have always been a lot of fun with you! Special thanks to Annariikka Roselli for being such a loud (and crazy) but great colleague and an amazing friend. There are many aspects of the Finnish culture that I would not have experienced without you! Your laugh and “oh oh oh you...French!!” will keep on resonating in my head! Among the spinning

team, I would also like to give thanks to: Yibo Ma, Shirin Asaadi and Simone Haslinger for their hard work! Being part of this team is not an easy thing, believe me! Thank you for sharing with me the highly stressful time of the never-ending demonstration runs!

I would like to warmly thank Seppo Jääskeläinen, Timo Ylönen, Christian Orassaari and the workshop group for their valuable and endless help with all the equipment in the spinning lab. The demonstration runs and regular public spinning lab tours would not have been possible without your fast assistance.

Many thanks to the laboratory technicians Rita Hatakka for her invaluable help in ordering the precious ionic liquid components, Minna Mäenpää for her assistance in GPC measurements and Marja Kärkkäinen for her extreme patience with the fiber testing.

I am grateful to all the support team members whom the enormous administrative work throughout these past 5 years could have been chaotic.

I would also like to express appreciation to all the incredible people I have met or work with during my stay at puu, in particular: Naveen Chenna, Marjaana Tanttu, Ramarao Abburi, Arcot Lokanathan, Elli Niinivaara, Alexey Khakalo, Eve Jutila, Anna-Maija Kostiainen, Saija Väisänen, Reeta Salminen, Katarina Dimic-Misic, Mindaugas Bulota and Agnes Stepan.

Special thought goes to the M-Club whose members are nowadays occupying different parts of the world. Marcelo, your Brazilian hip moves have blurred my eyes forever! Miro, your continuous super active mind will always astonish me! Mao, thank you for being an amazing person and such a great friend! You have left three years ago but your infinite support and encouragement in every situation have always pushed me forward.

I could not have been through the last 5 years without the endless support and amazingly enjoyable times spent with les Papetiers and Orléanais: Thomas, Romain, Elsa, Marion, Bertrand, Vincent, Marianne, Fufu, Guillaume, Coralie, Simon, Sandrine, Rémi, Benjamin and François. Thank you for reminding me how a real French should behave every time we meet! Deepest thanks to Thomas and Romain (or Romain and Thomas! Don't fight please!) for being here for me every time I need it.

Durante mis 20 minutos de dulzura... yo querría expresar mi enorme agradecimiento a Clara, Windi, Beñat y Victor por cada momento que compartimos juntos durante estos últimos 6 años. Su amistad me permitió seguir adelante aun cuando el futuro parecía difícil. Muchas gracias por estar ahí para mi!

Pour finir, un énorme remerciement à ma famille sans laquelle je n'aurais pas pu en arriver là. Merci pour votre présence et vos encouragements malgré mon caractère et comportement typiquement Michud(ien)!

Espoo, April 2016

Anne

List of publications

Paper I

Anne Michud, Michael Hummel, Simon Haward and Herbert Sixta. 2015. Monitoring of cellulose depolymerization in 1-ethyl-3-methylimidazolium acetate by shear and elongational rheology. *Carbohydrate Polymers*, 117, 355-363.

Paper II

Anne Michud, Marjaana Tanttu, Shirin Asaadi, Yibo Ma, Eveliina Netti, Pirjo Kääriäinen, Anders Persson, Anders Berntsson, Michael Hummel and Herbert Sixta. 2016. Ioncell-F: ionic liquid-based cellulosic textile fibers as an alternative to viscose and Lyocell. *Textile Research Journal*, 86(5), 543-552.

Paper III

Anne Michud, Michael Hummel and Herbert Sixta. 2015. Influence of molar mass distribution on the final properties of fibers regenerated from cellulose dissolved in ionic liquid by dry-jet wet spinning. *Polymer*, 75, 1-9.

Paper IV

Anne Michud, Michael Hummel and Herbert Sixta. 2016. Influence of process parameters on the structure formation of man-made cellulosic fibers from ionic liquid solution. *Journal of Applied Polymer Science, 133(30)*.
DOI: 10.1002/APP.43718

Author's contribution

Paper I

Anne Michud was responsible for the experimental design, performed the experimental work, analyzed the corresponding results and wrote the manuscript as principal author. Simon Haward contributed to the interpretation of the elongation rheology.

Paper II

Anne Michud was responsible for the experimental design together with the co-authors, produced and characterized the staple fibers together with Shirin Asaadi and Yibo Ma and wrote the manuscript as principal author. Marjaana Tanttu and Eveliina Netti produced the yarns and the final garments. Anders Persson and Anders Berntsson contributed to the production of the yarns.

Paper III

Anne Michud was responsible for the experimental design, performed the experimental work, analyzed the corresponding results and wrote the manuscript as principal author.

Paper IV

Anne Michud was responsible for the experimental design, performed the experimental work, analyzed the corresponding results and wrote the manuscript as principal author.

List of essential abbreviations

[EMIM]OAc – 1-ethyl-3-methylimidazolium acetate

[DBNH]OAc – 1,5-diazabicyclo[4.3.0]non-5-enium acetate

B-PHK – birch prehydrolysis kraft

CL – cotton linters

COP – cross-over point

DP – degree of polymerization

DR – draw ratio

DSC – differential scanning calorimetry

E-PHK – eucalyptus prehydrolysis kraft

G' – storage modulus

G" – loss modulus

IL – ionic liquid

MMCF – man-made cellulosic fiber

MMD – molar mass distribution

M_n – number average molecular mass

M_w – weight average molecular mass

NMMO – *N*-methylmorpholine *N*-oxide

NMR – nuclear magnetic resonance

PDI – polydispersity index

RTIL – room temperature ionic liquid

TGA – thermogravimetric analysis

Δn – birefringence

η_o – zero-shear viscosity

Contents

1. Introduction

The world population has been expanding by 1% annually on average over the last fifteen years to reach 7.2 billion today. This increase has had a direct impact on food and textile demands, which have been constantly rising also over recent years. Growing population prosperity has also become a key factor in driving the consumption of goods such as textiles and clothing. The consumption of fibers has strongly been driven by the advanced economies (Japan, Western Europe and North America), which currently have an annual textile consumption of around 25 kg per capita. However, the contribution to the textile consumption of emerging countries such as India, Indonesia, Pakistan, Bangladesh and Nigeria (currently 6.5 kg per capita) is expected to strengthen, attaining the level of the advanced economies by 2020 due to population prosperity growth (The Fiber Year 2015, Haemmerle 2011). Hence, larger fiber production will be needed in the coming years.

World fiber consumption attained 93.7 million tons in 2014, corresponding to an average textile consumption of 13.1 kg per capita. The 4.1% gain over the 2013/14 season in the world fiber market reflects the strong growth of man-made fibers (+4.9% over the 2013/14 season), which amounted to 63.2 million tons in 2014. Man-made fibers are represented by synthetic and cellulosic fibers that correspond to a share of 90.3% and 9.7%, respectively. Natural fiber consumption (such as cotton, bast and wool) also experienced an increase of 2.5% to 30.5 million tons in 2014. However, the natural fiber market, dominated by cotton accounting for 80%, has declined by 1.7% since 2010 (The Fiber Year 2015).

Cotton production is expected to stagnate or even shrink in the coming years, due to limited water availability in cotton-growing countries and the reduction of arable land in favor of food crops. Moreover, cotton production requires using fertilizers and pesticides to increase yield, which weaken the sustainability of cotton fibers (Haemmerle 2011, Eichinger 2011). In 2014, cotton production totaled 26.4 million tons but is predicted to slightly decline to 26 million tons by 2030 according to Haemmerle (2011). The same study envisions an annual fiber production of 133.5 million tons in 2030, with an estimated demand for cellulosic fibers of 44-49 million tons, of which only 26 million tons could be covered by cotton (Haemmerle 2011). This future so called *cellulose gap* cannot be currently filled with synthetic fibers, as their physiological performance does not match the performance of cellulosic fibers.

Man-made cellulosic fibers (MMCFs) are the best option to supplement cotton and fill the cellulose gap, as they offer similar properties of moisture management, providing absorbency and breathability to the body (Haemmerle 2011, Eichinger 2011). MMCFs also offer more sustainability than cotton, as the renewable resource wood does not compete with the cultivation of food crops and does not require any additional fresh water, fertilizer or pesticides (The Fiber Year 2015, Haemmerle 2011). In recent years, environmental awareness and societal considerations have risen, promoting MMCFs over synthetic fibers.

Man-made cellulosic fibers are presently produced mainly by the viscose process developed in the late 19th century and the Lyocell process, which emerged in the early 1990s as a more environmentally-friendly technology. Viscose fibers are the largest commercial type of MMCFs with a global production in 2014 of 4.8 million tons, accounting for 78% of the total MMCFs production (The Fiber Year 2015). Tencel®, which is the trade name of the Lyocell fiber produced by the Lenzing Group, amounts to about 220 000 tons per year.

Viscose and Tencel® fibers constitute the best substitute for cotton fibers, as they exhibit superior properties of moisture management and softness. They support a wide range of end-uses, from traditional apparel to technical textiles and non-woven materials (Eichinger, Eibl 1995, The Fiber Year 2015). The production of viscose fibers, which has undergone a decline since the emergence of synthetic fibers, showed a significant growth at the beginning of the 21st century due to increased demand from the developing industry in Asia. Nevertheless, the utilization of carbon disulfide as a cellulose derivatizing agent and the formation of highly toxic chemicals and gases in this process (which are harmful to labor forces and the environment) have reduced its attractiveness to covering the future need of MMCFs (North 2013, Bywater 2011). The Lyocell process, employing the direct cellulose solvent *N*-methylmorpholine *N*-oxide monohydrate (NMMO), is currently the only commercialized alternative to the viscose route. The NMMO-Lyocell process represents a more sustainable technology for the production of MMCFs, as the nearly-full recovery of the solvent permits a closed-loop production process (Harms 2013, Eichinger, Eibl 1995, Coulsey, Smith 1995).

Due to several side reactions and by-products formed by the cellulose-NMMO-water system, the NMMO-Lyocell process requires a stabilizer at a relatively high processing temperature to reduce the chance of dangerous runaway reactions. However, this does not guarantee a risk-free process (Rosenau, Potthast et al. 2001). Thus, there remains a need for a more cost-effective and eco-efficient production method of MMCFs.

The present study focuses on producting a new type of MMCFs from an ionic liquid (IL) solution, the so called Ioncell-F(iber). This study explores the different steps in the entire production chain, from the dissolution of cellulose in ionic

liquid to the production of apparel exhibited in Figure 1.1. but does not include the IL-recovery step.

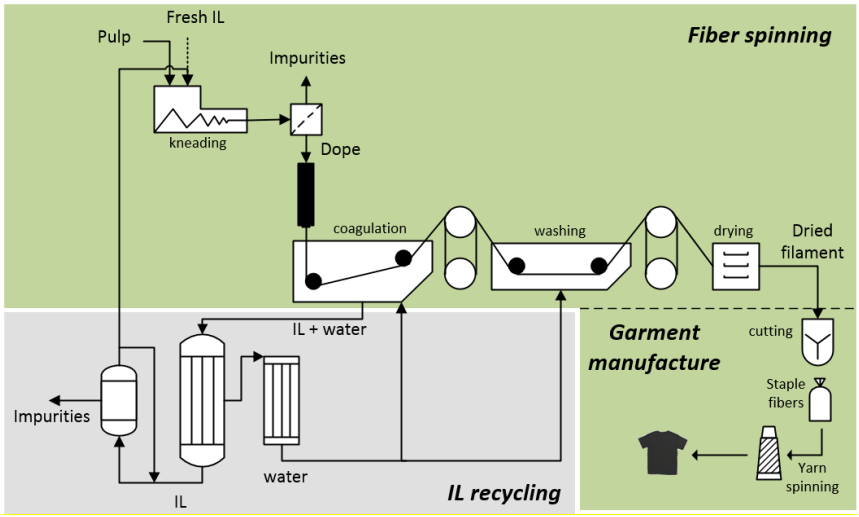

Figure 1.1. Process scheme.

A major part of this work was conducted with the non-commercialized ionic liquid 1,5-diazabicyclo[4.3.0]non-5-enium acetate ([DBNH]OAc) developed at the University of Helsinki. This thesis work began with utilization of the imidazole-based IL, 1-ethyl-3-methylimidazolium acetate ([EMIM]OAc]), which was heavily promoted due to its low viscosity, low melting point and ease to dissolve cellulose. Despite its excellent ability to dissolve cellulose, however, [EMIM]OAc showed very poor spinnability. The study therefore continued by using the promising [DBNH]OAc.

The main aspects investigated in this study were summarized in four papers as reported in Figure 1.2. **Paper I** evaluates the thermal behavior of cellulose in the ionic liquid [EMIM]OAc by monitoring the depolymerization of cellulose through the determination of the shear and elongational viscosity of cellulose/[EMIM]OAc solutions stored at different temperatures and times. **Papers III** and **IV** look into the processability of [DBNH]OAc solutions and the direct impact of solution composition and spinning parameters on the properties of the resulting fibers. The influence of the molar mass distribution (MMD) of cellulose on the rheological behavior of the polymer solution, stretching ability of the extruded filament, and the properties of the resulting fibers were explored in **Paper III**. **Paper IV** examines the effect of the principal process parameters on the structural and mechanical properties of fibers produced from [DBNH]OAc solutions. In **Paper II**, the suitability of Ioncell-fibers for textile applications was investigated through the production of knitted and woven garments. In this paper, the manufacture of these apparels, from the production of the Ioncell staple fibers to the knitting or weaving step is explored. This paper

also compares Ioncell-fiber performance as a potential alternative to the current viscose and Tencel® fibers.

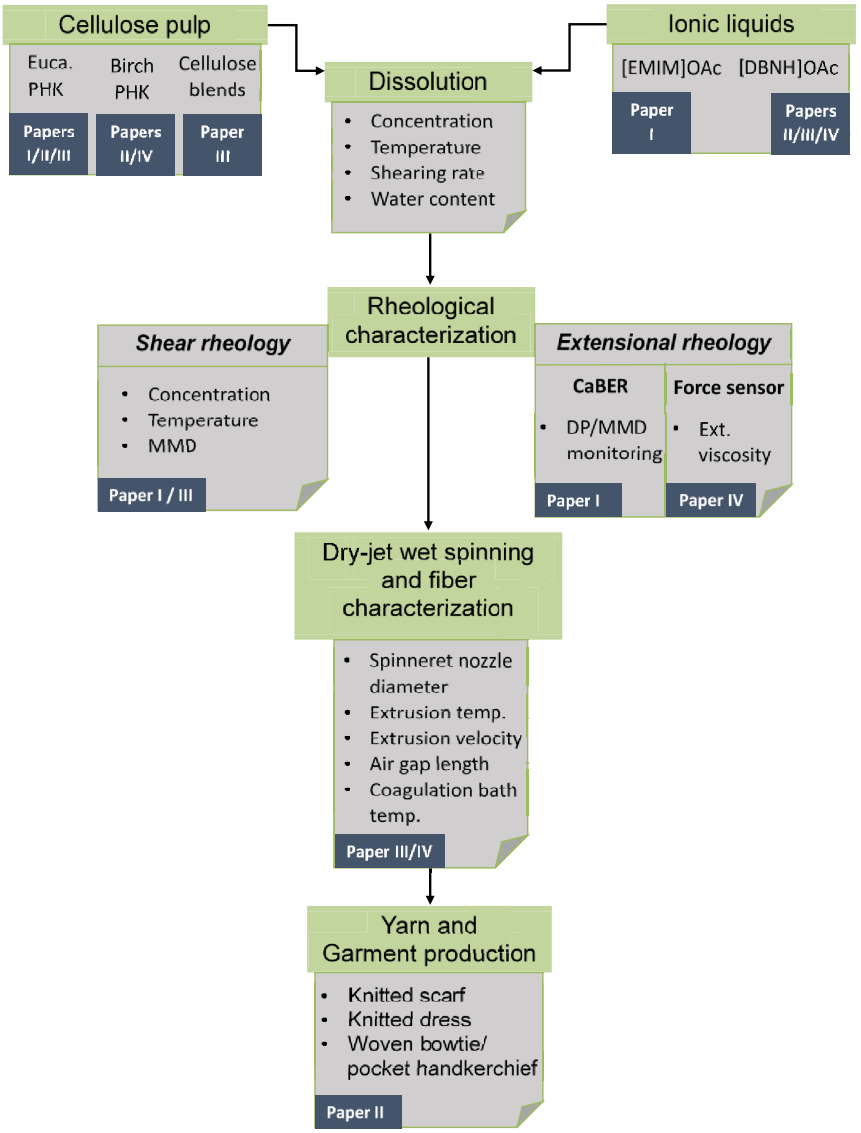

Figure 1.2. Visualized summary of the thesis.

2. Research questions

This work started in 2011 based on literature that claim the possibility to spin cellulose filament from ionic liquid solution. However, none of the existing publications was reporting experimentations using appropriate spinning equipment. This work was dedicated to the evaluation of the true potential of ionic liquid spinning for the production of man-made cellulosic fibers on an industrial scale. Within this scope, fundamental process aspects have been investigated:

- Development of an efficient method for cellulose dissolution and evaluation of its thermal stability in ionic liquid

- Suitability for fiber spinning of ionic liquids previously described in literature

- Development of a spinning window to achieve continuous spinning of cellulose filament using [DBNH]OAc as solvent

- Assessment of the extensional viscosity of cellulose/IL solution

- Establisment of a relationship between the spinnability of a cellulose/IL solution, its viscoelastic properties and the molar mass distribution of the dissolved cellulose

- Production of competitive textile fibers for the manufacture of garments

3. Background

3.1 The complexity of cellulose structure

Cellulose, being the major component of plants and algae, constitutes the most abundant natural polymer present on earth. Wood, cotton fiber and cotton linters constitute the principal sources of cellulose employed industrially. The linear structure of cellulose consists of D-glucopyranose repeating units linked by β-1,4-glycosidic bonds, where each anhydroglucose unit is rotated 180° with respect to its neighbor. The degree of polymerization (DP) of cellulose, which is the number of repeating units of glucose, depends on its source. In wood, the DP is approximately 10 000 glucopyranose units while an amount of 15 000 is estimated in native cotton (O'Sullivan 1997). Each monomer involves three hydroxyl groups, secondary on C2, C3 and primary on C6, which, due to their equatorial orientation, contribute to the formation of intra and intermolecular hydrogen bonds along and between the cellulose chains, respectively. Intramolecular bonds give the stiff nature of the cellulose chains and the intermolecular bonds are responsible for the arrangement of the polymer chains in sheet structure. These sheets are stacked on top of each other due to CH – O interactions between the axial CH groups in sugar rings and the oxygen atoms in ether bonds and hydroxyl groups of two different sheets. Van der Waals (vdW) interactions between cellulose sheets also contribute to the formation of a strong network. The intersheet bonding, which appears to be the most stable interaction among these three, lead to the formation of a robust three-dimensional crystal structure (Gross, Chu 2010, Cho, Gross et al. 2011).

Four major polymorphs of cellulose (I, II, III and IV) have been distinguished by x-ray diffraction, wide-angle x-ray scattering and ^{13}C-NMR examination, with cellulose I and II being the most investigated forms (Kadla, Gilbert 2000, O'Sullivan 1997). Cellulose I corresponds to the native cellulose found in most plants and is a composite of two distinct forms I_α and I_β. The latter corresponds to the predominant form in wood and accounts for approximately 60 to 70% of the cellulose I crystal structure (Atalla, Vanderhart 1984). Cellulose I_α has a triclinic unit cell containing one chain whereas cellulose I_β has a monoclinic unit cell containing two parallel chains. In the monoclinic unit cell, the origin chain is located at the corner of the unit parallel to the *c* axis direction and the center chain is positioned at the center of the a/b plane and is translated in the *c* axes direction by about $c/4$ with respect to the origin chain (Nishiyama, Langan et

al. 2002, O'Sullivan 1997). Cellulose II is obtained from cellulose I by dissolution/regeneration or mercerization processes. Cellulose I exhibits a parallel chain orientation while cellulose II shows an anti-parallel orientation, which results in differences in the hydrogen bond patterns. The pattern of the hydrogen bond network has been actively investigated but described differently by several authors (Gardner, Blackwell 1974, Kadla, Gilbert 2000, O'Sullivan 1997, Nishiyama, Langan et al. 2002, Langan, Nishiyama et al. 1999). The hydrogen bond patterns of cellulose I and II suggested by Nishiyama, Langan and Chanzy from neutron fiber diffraction analysis are depicted in Figures 3.1 and 3.2, respectively. The conformation of the C6 hydroxymethyl group throughout the cellulose chain plays a major role in the hydrogen bond pattern of cellulose I and II. There are three possible orientations of the hydroxyl constituent to the pyranose ring: trans-gauche (tg), gauche-trans (gt) and gauche-gauche (gg). The closeness of the oxygen and carbone substituents explains the differences in energy and stability between these conformations (O'Sullivan 1997). The widely described tg conformation of cellulose I_β favors a hydrogen bond pattern (Figure 3.1) consisting of the intramolecular bonds O5-OH3 in center and origin chains, OH2-O6 in center chains and OH2-O6 involving O1 as acceptor in origin chains. The intermolecular hydrogen bond network consists of OH6-O3 in sheets containing origin chains and OH6-O3 involving O2 as acceptor in sheets containing center chains (Nishiyama, Langan et al. 2002). Neutron diffraction study of cellulose II demonstrated that origin and center chains have different conformations but a common gt conformation of the hydroxymethyl groups which favors the intermolecular hydrogen bond between O6 atoms (Figure 3.2). An intramolecular hydrogen bond OH3-O5 involving O6 as acceptor is observed in both chains. Intermolecular hydrogen bonds OH2-O6 in sheets containing only origin molecules and OH6-O2 in sheets containing only center molecules are distinguished. In sheets containing both origin and center chains, intermolecular hydrogen bonds OH2-O2 and OH6-O6 involving O5 and O3 as acceptors are observed (Langan, Nishiyama et al. 1999).

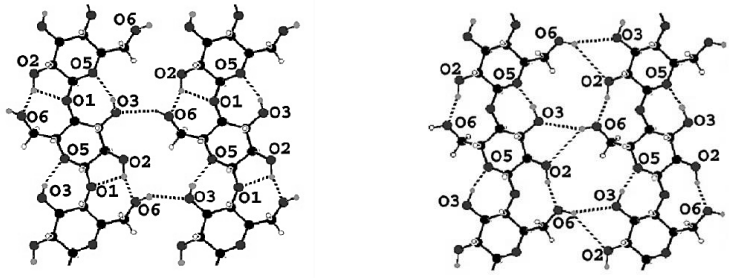

Figure 3.1. Hydrogen bond pattern of cellulose I. Left: origin chains, right: center chains (Nishiyama, Langan et al. 2002).

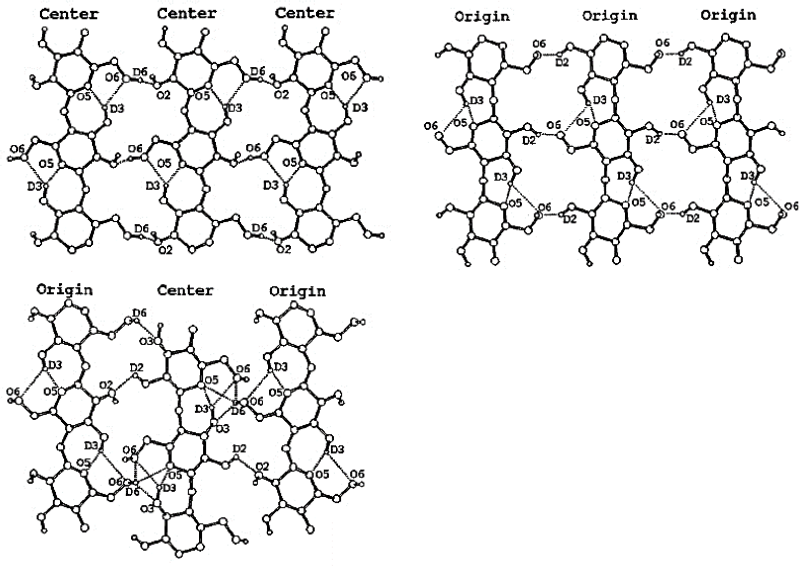

Figure 3.2. Hydrogen bond pattern of cellulose II (Langan, Nishiyama et al. 1999).

Cellulose is known to be insoluble in water and in conventional organic solvents. The few solvents that show the capability of dissolving cellulose do not present clear common properties. The complex network of intra- and intermolecular hydrogen bonds between cellulose molecules is frequently referred as the principal factor for cellulose insolubility. Following this statement, a solvent is suitable for cellulose dissolution if it is capable of disrupting the extensive hydrogen bond structure by interacting itself with cellulose (Olsson, Westman 2013a, Lindman, Karlström et al. 2010, Zhang, Ruan et al. 2002). However, several studies disagree and point out the important role of the amphiphilic nature of cellulose and of the stability of the intersheet interactions in cellulose network to explain its recalcitrance toward dissolution.

As previously mentioned, the complex structure of cellulose I is built via a network of hydrogen bonding and vdW interactions. The intrachains, O5-OH3 and OH2-O6, the interchains O6-O3 within cellulose layers, and the CH-O and vdW interactions between the cellulose sheets exhibit different strength and stability. The interaction O5-OH3 occupies a well-defined location which makes the surface of O3 unreactive and enhance the stability of the hydrogen bond. The interaction between OH6 and O3 of two chains plays a significant role in maintaining the structural integrity of cellulose. However, the rotational ability of C6 favors the reactivity of the OH6 group which can undergo the disruption of the crystallinity and thus facilitate cellulose dissolution (Nishiyama, Langan et al. 2002, Gross, Chu 2010). Gross et al. report the important role of intersheet interactions in the recalcitrance of cellulose toward dissolution. They describe the CH-O bonds between cellulose sheets, besides being the most abundant interactions within the network, as stronger, more robust and less flexible. The superior stability of these interactions originates from the geometry in the crystal structure

of cellulose: a close-to-linear angle and a short H-O distance. CH-O interactions are not dependent on solvent exposure while intra- and intermolecular chains are sensitive to it due to the lack of molecular packing and competition with the solvent to form hydrogen bonds. However, CH-O intersheet interactions involving C6 exhibit a more pronounced diminution in strength due to higher flexibility compared to the CH-O bonds which do not involve C6. The latter participate to the high integrity and low flexibility of the network and affect significantly the cellulose dissolution. Furthermore, a decrease in interaction strength is observed at the outmost chains wing to the solvent exposure while the interactions located inward are not noticeably affected (Gross, Chu 2010). Another study from Lindman et al. highlights the amphiphilic nature of cellulose and the presence of hydrophobic interactions within the cellulose network. According to this study, the cellulose sheets demonstrate different polarity due to the hydrophilic and hydrophobic parts which undergo conformation adjustment to reduce the contact between water and the hydrophobic regions. He concluded that an amphiphilic solvent would promote cellulose solubility (Lindman, Karlström et al. 2010, Medronho, Romano et al. 2012). Burchard, in response to the Lindman hypothesis, asserts the role of primary (C6) and secondary (C2 and C3) OH-groups in the hydrophobicity of the cellulose network, the less hydrophilic primary group being the origin of the hydrophobic behavior. In the same discussion, Blackwall emphasizes the importance of hydrophobic stacking forces between the CH-O groups of cellulose sheets in cellulose recalcitrance. They point out that a solvent needs to break both types of bonds to successfully dissolve the complex cellulose network (Glasser, Atalla et al. 2012).

3.2 Cellulose solvents

Despite the cellulose recalcitrance toward dissolution in water and many other media, several systems show the ability to dissolve cellulose. These solvents can be classified into different categories, namely indirect or derivatizing solvents, complexing solvents and direct or non-derivatizing solvents.

Indirect solvents require the formation of a cellulose derivative, which is then dissolved. The dissolution of cellulose via the derivatization of cellulose with carbon disulfite (CS_2) belongs to this group. This procedure is called the viscose process and constitutes the most successful cellulose dissolution route that has been industrially developed so far for the production of man-made cellulosic fibers. In this process, the dissolution of cellulose is achieved by the formation of a derivative, which implies the requirement of several steps prior to the actual dissolution and regeneration of cellulose into filaments. The xanthation of cellulose is executed by the reaction of CS2 with the C2, C3 and C6 hydroxyl substituents. The derivatization on C2 and C3 is kinetically favored over the C6 substitution. The following dissolution of the cellulose xanthate is conducted in dilute sodium hydroxide solution at low temperatures. The resulting viscose solution is aged to promote an even distribution of CS_2 on cellulose chains, filtered and deaerated before being spun in sulfuric acid to filaments (Woodings 2001).

Complexing agents, containing a transition metal and an amine or ammonium component, form a second group of cellulose solvents. The most common ones are cuen ($[Cu(H_2N(CH_2)_2NH_2](OH)_2$), nitren ($Ni[NH_2CH_2CH_2)N](OH)_2$) or cuoxam ($[CuNH_3)_4](OH)_2$). This class of solvent dissolves cellulose by deprotonation at C2 and C3 positions of the anydroglucose units and coordinatively binding to the hydroxyl groups. Several complex agents, such as cuen, can also interact with cellulose through Coloumb interactions. The cuproammonium process, employing cuoxam as dissolving agent, is the second process that has been developed for the regeneration of cellulose but plays presently a minor role in the industry due to environmental concerns and the presence of the already well-established viscose process on the market (Olsson, Westman 2013a, Liebert 2010).

The third route that has been industrially developed and is presently in use for the production of man-made cellulosic fibers consists of the direct dissolution of cellulose in *N*-methylmorpholine *N*-oxide (NMMO), depicted in Figure 3.3.

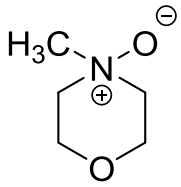

Figure 3.3. Structure of *N*-methylmorpholine *N*-oxide.

By using direct solvents, cellulose does not need to be chemically modified prior to dissolution. NMMO-monohydrate (13 – 15% water) has proven to be an efficient cellulose solvent without the requirement of prior derivatization or activation. The dissolution mechanism is still not fully understood but the formation of hydrogen bond complexes between the oxygen of the strong N – O dipoles in NMMO and the compounds containing hydroxyl groups, such as water and cellulose, is expected to occur. The dissolution procedure, first, consists of mixing cellulose in NMMO with a large excess of water to favor efficient mixing and swelling. The dissolution starts when the surplus of water is removed via the use of high vacuum and elevated temperature and the NMMO-monohydrate is reached. The regeneration of cellulose into filaments is performed after filtration and deaeration of the NMMO solution which is spun by dry-jet wet spinning into a water bath. However, the success of NMMO is tarnished by the thermal instability of the amine oxide which implies the use of stabilizer to prevent the radical degradation of NMMO (Woodings 2001, Liebert 2010, Olsson, Westman 2013a, Fink, Weigel et al. 2001, Rosenau, Potthast et al. 2001).
Another category of attractive direct cellulose solvents are ionic liquids, which have been thoroughly examined since 2002.

3.3 Ionic liquid as cellulose solvent

Ionic liquids (ILs) are a group of salts which are liquid at temperatures below 100 °C due to the presence of bulky and unsymmetrical ions with a delocalized charge. They comprise an organic cation and an organic or inorganic anion. Room temperature ionic liquids (RTILs) are ILs that have a melting point below 25 °C (Pinkert, Marsh et al. 2009, Cao, Wu et al. 2009, Rogers, Seddon 2003). Figure 3.4 depicts the principal cations and anions employed for the synthesis of cellulose-dissolving ILs.

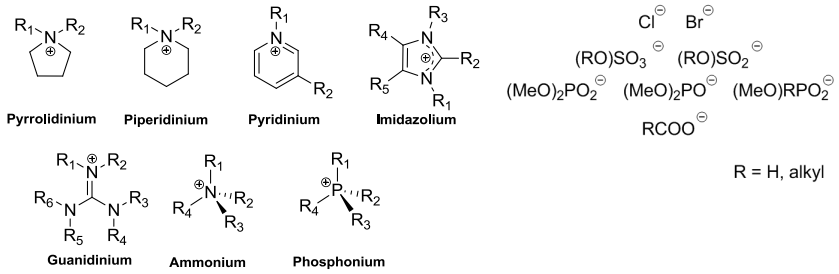

Figure 3.4. Most common cations and anions found in cellulose-dissolving ILs.

The first successful attempt to dissolve cellulose in ILs was achieved by Graenacher in 1934 who discovered that molten *N*-ethylpyridinium chloride, in the presence of nitrogen containing bases could dissolve cellulose (Graenacher 1934). The past few years have witnessed a large interest toward the applicability of ILs as new media for lignocellulosic processing since Swatloski et al. reported in 2002 the dissolution of cellulose in some alkyl substituted imidazolium RTILs (Swatloski, Spear et al. 2002). The attractive properties of ILs such as low vapor pressure, enhanced chemical and thermal stability and non-flammable properties, explain the recent surge in research seeking for substituting the traditional volatile organic industrial solvents (Rogers, Seddon 2003, El Seoud, Koschella et al. 2007). The large panel of anions and cations offers a variety of physical properties that make them suitable for a large field of applications. In addition to the ability of ILs to dissolve cellulose for subsequent filament shaping, they feature good properties as reaction media for cellulose modification (Pinkert, Marsh et al. 2009, Zhu, Wu et al. 2006, Feng, Chen 2008, Heinze, Dorn et al. 2008, El Seoud, Koschella et al. 2007).

According to Pinkert et al., ILs possess strong capacity of dissolving cellulose due to their high polarity and hydrogen bond basicity (Pinkert, Marsh et al. 2009). The capability of ILs to dissolve cellulose can be estimated by evaluating the hydrogen bonding and polarizability properties of the solvent. The empirical Kamlet-Taft model has been frequently employed to predict the solubility of cellulose in ILs. The Kamlet-Taft parameters β, α and π* describe the hydrogen bond basicity, the hydrogen bond acidity, and the solvent interactions through dipolarity and polarizability, respectively. These parameters are determined by assessing the UV-Vis spectra of dyes when dissolved in the tested solvent (Olsson, Westman 2013a, Brandt, Gräsvik et al. 2013, Hauru, Hummel et al. 2012,

Doherty, Mora-Pale et al. 2010). Crowhurst et al. reported that π* varies with both anion and cation, α depends mainly on the cation and β mainly on the anion. They concluded that ILs are polar solvents that can act both as hydrogen bond donors and hydrogen bond acceptors (Crowhurst, Mawdsley et al. 2003). Hauru et al. introduced the net basicity (β-α) as a more accurate parameter to describe the dissolution ability of ILs. They demonstrated that ILs having parameters in the regions of $0.35 < \beta-\alpha < 0.9$ and $0.80 < \beta < 1.20$ favored the dissolution of cellulose (Hauru, Hummel et al. 2012).

The dissolution mechanism of cellulose in ILs is not fully understood yet. Some studies report the dissolution to involve the breaking of the hydrogen bond complexes of the cellulose network through the formation of electron donor-electron acceptor complexes between the IL entities and the oxygen and hydrogen atoms of the cellulose hydrogen bonds (Feng, Chen 2008, Cao, Wu et al. 2009). The interactions between the hydrogen of the hydroxyl groups of cellulose and the anion, and between the oxygen atom of the hydroxyl groups and the cation were observed by nuclear magnetic resonance (NMR) studies by Singh et al (Singh, Simmons 2013). The capability of anions to disrupt hydrogen bonding and dissolve cellulose is related to their basicity and dipolarity. Higher basicity and dipolarity enhance the hydrogen bond accepting ability of the anions (Swatloski, Rogers et al. 2003, Wang, Gurau et al. 2012, Brandt, Gräsvik et al. 2013, Sun, Rahman et al. 2009). However, the role of the cation in the dissolution of cellulose is still subject of debate. Several studies suggest that the cation does not directly interact with the hydroxyl group of cellulose but rather contributes indirectly to the dissolution process depending on its chain length, size, polarizability and functional groups. Long chains on the cation reduce cellulose solubility. Large aromatic cations show the ability to shield the formed anion-cellulose complexes. The high polarizability of the cation ring favors the formation of hydrogen bonds between the anions and cellulose. The presence of functional group on the cation, such as hydroxyl group, can affect the dissolution process by competing with cellulose for hydrogen bond donation to the anion (Brandt, Gräsvik et al. 2013, Wang, Gurau et al. 2012, Mäki-Arvela, Anugwom et al. 2010).

The purity of ILs is of great importance for the efficiency of cellulose dissolution or derivatization. The presence of IL-derived by-products, resulting from IL thermal degradation, synthesis or recovery cycle can strongly affect the performance of the processes. Rosenau et al. demonstrated that the system cellulose/1-alkyl-3-methyl-imidazolium ionic liquid is not inert. 1-alkyl-3-methyl-imidazolium cations react at its C-2 position with the reducing end of cellulose forming a carbon-carbon bond. This reaction is catalyzed by basic compounds, mainly imidazole, formed by thermal degradation (Schrems, Ebner et al. 2010).

3.4 Rheological characterization of cellulose/ionic liquid solution for process purpose

The rheological behavior of polymer solutions plays a significant role in many industrial operations where a rapid change of flow is involved. In dry-jet wet fiber spinning, the solution is first extruded through a spinneret, the resulting fluid filaments are then stretched in an air gap, regenerated in a coagulation bath and finally collected. The polymer solution is subjected to shear stress when passing through the spinneret nozzles and extensional stress when stretched in the air gap. The assessment of the shear and extensional behavior of ionic liquid solutions is therefore fundamental to predict their behavior under the different flow conditions and successfully process them by dry-jet wet spinning (Plog 2005).

3.4.1 Behavior of ionic liquid solution under shear stress

The establishment of a stable extrusion of an ionic liquid solution through a spinneret relies on the viscoelastic properties of the extruded polymer solution. The dissolved cellulose chains form an interlooped and entangled network with temporary knots, which responds differently when subjected to increasing shearing stress. At low shear rate, the molecule network conserves its minimum energy-state, the polymer molecules have time to avoid the imposed deformation. Under these conditions, the entanglement points slowly move and relax by sliding along each other. The polymer solution exhibits a viscous flow behavior. On the contrary, when applying high shear rate, the chain ties behave like fixed network joints, the molecule chains are elastically stretched and orient in the direction of the shearing force. The deformation energy that is absorbed and stored by the elastic deformation is then partly recovered during the relaxation phase when the polymer chains retract to their relaxed state (Gebhard 2004, Chen, Zhang et al. 2009). The viscoelastic properties of a polymer solution can be evaluated via dynamic measurements by applying a small amplitude oscillatory shear. In this technique, the small amplitude deformation applied to the tested solution prevents the destruction or the fracture of the chain network at high shear rate. According to the empirical Cox-Merz rule, the resulting complex viscosity can be used to predict the steady shear viscosity, which is difficult to measure at high shear rate due to the sample fracture. The Cox-Merz rule states that the complex viscosity is the same as the steady shear viscosity at equal values of frequency and shear rate for polymeric systems (Gebhard 2004). Cellulose/IL solutions of medium concentration (10-15 wt-%) appear to obey to the Cox-Merz rule (Haward, Sharma et al. 2012, Rudaz, Budtova 2013).

The shear viscosity of polymer melts depends on the applied deformation rate and shows a shear thinning behavior at increasing shear rate. At low shear rate, the entanglement points between cellulose chains have time to slip past each other, the shear viscosity thus does not vary and a plateau is observed. The zero-shear viscosity, corresponding to the shear viscosity at infinitesimal small strain, can be extracted from this steady state domain. Dynamic measurements

also provide the evolution of the viscous and elastic components of the polymer solution as a function of frequency. The storage modulus, G', corresponds to the part of the energy that is stored elastically whereas the loss modulus, G'', refers to the part of the energy that is dissipated through viscous flow (Plog 2005). At low frequency, the loss modulus shows higher values than the storage modulus. The polymer solution behaves thus like a viscous solution as the inserted energy is dissipated. At a certain frequency, the storage modulus exceeds the loss modulus which implies a change in the solution structure toward elastic behavior. This reverse in properties is observed via a cross-over point (COP) between the loss and storage moduli curves.

The shear behavior of cellulose/IL solutions is strongly influenced by the temperature of the solution and the DP, the molecular mass distribution (MMD) and the concentration of the dissolved cellulose. An increase in cellulose concentration or DP results in a denser cellulose network with more entanglement points. The polymer chains exhibit a restriction in motion, the fluidity of the solution is reduced and behaves more like an elastic solid. The COP between the loss and the storage moduli is shifted to lower frequencies, the elastic domain is widened and the viscous domain is narrowed. The shear thinning phenomenon observed in the shear viscosity is also more pronounced. On the contrary, a rise in temperature favors the molecule chains to move more freely, the rigidity of the solution decreases which results in an increase of the flow-ability. The viscous properties predominate at higher temperatures and the COP is shifted to higher frequencies (Sammons, Collier et al. 2008b, Collier, Watson et al. 2009, Chen, Zhang et al. 2009, Lu, Cheng et al. 2012, Golzar 2004).

3.4.2 Behavior of ionic liquid solution under extensional stress

Even though shear characterization is the most established rheological method, the assessment of the extensional or elongational behavior of a polymer solution is essential to investigate when stretching operations are involved in their processing. Polymer solutions exhibiting similar shear properties do not necessarily demonstrate comparable elongational properties (Collier, Romanoschi et al. 1998, Baird 1999). In a shear-free elongational flow, the polymer chains of a viscoelastic solution are stretched without being rotated or sheared. The formation of stable filaments in the air gap strongly depends on the response of the fluid elements to the rate and extent of the extensional deformation.

Capillary break-up extensional rheology (CaBER) is one method to assess the extensional rheological properties of fluids such as polymer solutions. This technique mimics the deformation experienced by the thread in the air gap by applying an axial step-strain to a small amount of solutions. The observation of the thinning and eventual break-up of the fluid filament in a shear-free uniaxial extensional flow under the combined action of viscous, elastic and capillary forces permits the extraction of the fluid relaxation time and apparent elongational viscosity (Rodd, Scott et al. 2005, McKinley, Tripathi 2000, Haward, Sharma et al. 2012). The filament self-thinning can be divided into four regimes

due to the set of forces which balance each other. In the first regime (I), the fluid cylinder is exposed to gravitational forces which are superimposing the capillary forces and distort the assumed axial symmetry around the mid-plane of the filament thread. In the second regime (II), the polymer solution exhibits Newtonian-like behavior, the filament diameter decreases slowly and linearly with time. The capillary forces γ/R (surface tension γ and filament radius R) that drive the filament thinning are balanced by the material's viscous tensile stresses $\eta_E\dot{\varepsilon}$ (apparent extensional viscosity η_E and extension rate $\dot{\varepsilon}$), that predominate the elastic tensile stresses. The filament diameter is still large, the extension rate $\dot{\varepsilon}$ is low and the cellulose chains are not stretched yet. In the third regime (III), the filament thinning is controlled by a visco-capillary balance of the capillary pressure and the viscous stresses present in the filament. However, the polymer solution shows an extensional thinning due to the higher surface pressure and thus extension rate. An increase in the disentanglement and orientation of the polymer chains is noticed in this regime. The onset of the elasto-capillary balance is observed in the fourth regime (IV) with the elastic stresses prevailing the viscous stresses within the filament and balancing the action of the capillary pressure. The diameter decay at this stage is described by an exponential function. This regime occurs at very small diameters close to breakup (Anna, McKinley 2001, Clasen 2010, Stelter, Brenn et al. 2002). The elasto-capillary thinning regime enables the determination of the relaxation time and the final extensional viscosity of the fluid. A Hencky strain hardening is observed at high strain, which corresponds to the increase of the elongational viscosity of the polymer solution due to the orientation of the polymer chains at high deformation during regime III (Haward, Sharma et al. 2012, Clasen 2010, Anna, McKinley 2001).

However, CaBER measurements show limitations in the assessment of the extensional behavior of highly viscous 13 wt-% cellulose/ionic liquid solutions at temperature of 70-80°C. The very long fluid thread decay after the axial step-strain do not allow an accurate determination of the elongational viscosity. A method to determine the elongational viscosity of a fluid during spinning has been developed by Boerstoel for cellulose solutions in super-phosphoric acid (Boerstoel 1998). The extensional viscosity is calculated via the online measurement of the tension force acting on the filament tow exiting the coagulation bath as a function of the air gap length. (Boerstoel, Maatman et al. 2001, Boerstoel 1998). The tension force is derived from the measurement of the radial forces acting on a strain gauge based force sensor placed at the exit of the coagulation bath. In this method, Boerstoel makes the following simplifications on the fluid behavior in the air gap:

- The velocity at the bath surface v_1 equals the take-up velocity v_{tu}.
- The flat velocity profile settles immediately after the fluid leaves the capillary.
- The occurrence of a die swell is ignored.

In the force balance, reported in Equation (1), Boerstoel assumes the gravitational (F_{grav}), friction (F_{fric}), surfacial (F_{surf}) and inertial (F_{iner}) forces to be small for high viscous materials compared to the external (F_{ext}) and rheology (F_{rheo}) forces. In that case, the external force balances the rheological force, as seen in Equation (2) (Boerstoel 1998).

$$F_{ext} + F_{grav} = F_{rheo} + F_{iner} + F_{surf} + F_{fric} \quad (1)$$

$$F_{ext} = F_{rheo} \quad (2)$$

The extensional properties of ionic liquid solutions are strongly influenced by the concentration, DP and MMD of cellulose and temperature at which the deformation is performed. An augmentation in cellulose concentration or DP favors the formation of an entanglement network which causes the increase of the elongational viscosity. Higher concentration also affects the relaxation time of the polymer chains and strengthens the elastic properties of the solution, which are of great importance for the formation of stable filaments in the air gap (Clasen, Verani et al. 2004, Clasen, Petri 2005). On the contrary, the elongational viscosity decreases with the increase in the process temperature and the strain rate thinning is more pronounced (Haward, Sharma et al. 2012, Sammons, Collier et al. 2008a, Petrovan, Collier et al. 2001).

3.5 Regeneration of cellulose into filaments

The name Lyocell is a generic name for cellulose fiber obtained by an organic solvent spinning process. The term “organic solvent” means here essentially a mixture of organic chemicals and water, and “solvent spinning”, the dissolution and spinning without the formation of a derivative (BISFA 2009). The processing of ionic liquid solutions by dry-jet wet spinning for the production of MMCFs is a recent field of research which shows potential as industrial application (Swatloski, Rogers et al. 2003, Hermanutz, Gähr et al. 2008, Kosan, Michels et al. 2008). The Ioncell fibers belong to the category of Lyocell fibers, provided that they are produced commercially.

3.5.1 Dry-jet wet spinning of ionic liquid solution

The formation of ionic liquid-based fibers by dry-jet wet spinning consists of the extrusion of a cellulosic polymer solution at mild temperature through a spinneret into an aqueous coagulation bath via an air gap. The solidified filaments are subsequently washed in water, dried and collected as endless filaments. Figure 3.5 illustrates the extrusion, stretching, coagulation and collection steps. Along the spinning line, the forming fibers are subjected to continuous structural changes, cooling, relaxation, coagulation, crystallization and drying.

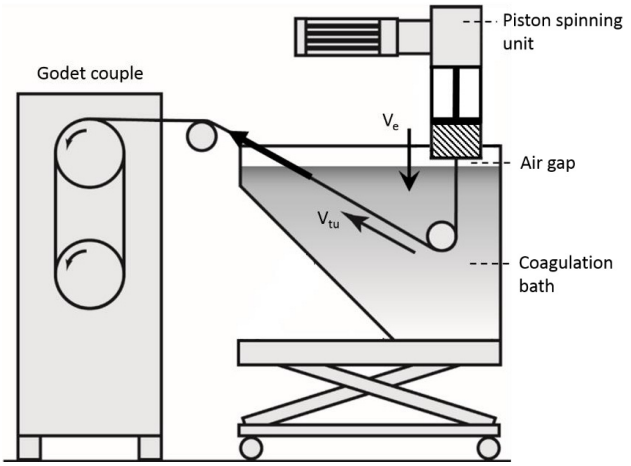

Figure 3.5. Simplified dry-jet wet spinning unit. V_e: extrusion velocity and V_{tu}: take-up velocity.

The shaping of the viscoelastic dope starts in the spinneret when the solution travels through the capillaries. The cellulose chains are subjected to shear deformation, which pre-orient them. However, when the fluid filament exits the capillary, abrupt changes occur in the boundary conditions as the fluid enters a shear-free zone. An immediate relaxation of the cellulose chains occurs which attenuates the orientation created by the spinneret flow. This can lead to an increase of the fluid diameter called die swell (Fink, Weigel et al. 2001, Ziabicki 1976). This phenomenon is over-compensated by the stretching of the viscous filaments in the air gap when pulled down through the coagulation bath by means of a godet couple. Figure 3.6 illustrates the formation of the die swell and the subsequent drawing of the fluid filament in the air gap when exiting the spinneret capillary. The cellulose chain orientation develops in the air gap due to the extensional flow created when drawing the filament. The elongation of the steady-state viscoelastic thread is not a purely extensional flow. The fluid filament is subjected to several forces which balance each other, also depicted in Figure 3.6. The gravimetric and the external take-up forces, which are constant along the thread path, are defined as deformation forces. The inertia force due to the acceleration of the fluid from the extrusion velocity, the friction force between the filament surface and the surrounding spinning medium, the rheological force associated to the viscoelastic behavior of the fluid and the surfacial force constitute the retarding forces (Fourné 1999, Ziabicki 1976). Figure 3.7 represents the orientation mechanism of the polymer chains in the drawing zone. The relaxed, non-oriented and randomly arranged cellulose chains are oriented under extensional tension (Fourné 1999). The extent of the alignment of the polymer chains along the longitudinal axis of the fiber is controlled by the amount of stretching applied to the filaments. The latter is defined by the draw ratio, corresponding to the ratio of the velocity of the take-up godet to the extrusion velocity (v_{tu}/v_{ex}). Due to the take-up force, the diameter of the fluid thread decreases along the air gap leading to an increase in stress within the filament and a development of the chain orientation, promoting the formation

of a closely packed cellulose network in the coagulation bath (Gordon Cook 1984, Ziabicki 1976, Woodings 2001). Mortimer et al. demonstrated that the filament diameter levels off after a certain distance, also called draw length, after which the fluid is too cold and viscous to undergo further orientation. The increase in stress within the elongated fluid also leads to a diminution of the potential relaxation of the cellulose chains, which is a phenomenon competing with the orientation process (Mortimer, Peguy 1994, Mortimer, Peguy 1996a). The same study reported the evolution of the fiber orientation through the whole spinning process and demonstrated that the chain orientation takes place mainly in the air gap and during the solidification of the filament in the coagulation bath. Only slight increase in orientation occurs during drying, due to the shrinkage of the structure and further crystallization (Mortimer, Peguy 1996a).

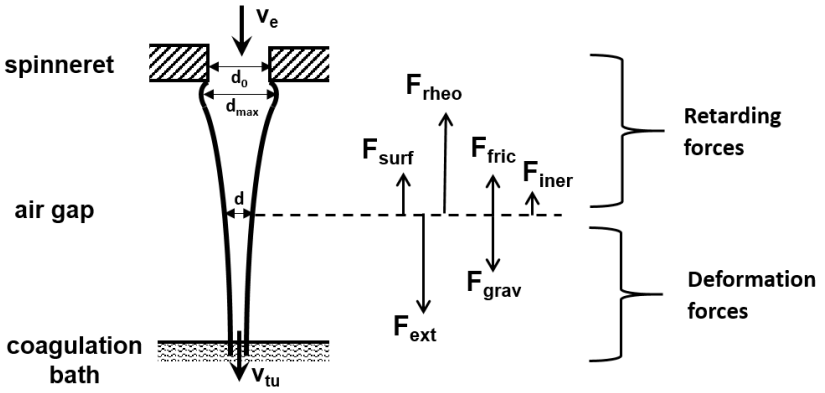

Figure 3.6. Orientation mechanism of polymer chains in the drawing zone.

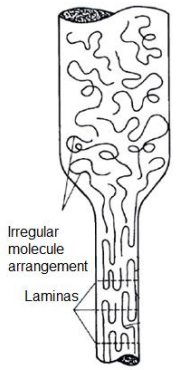

Figure 3.7. Orientation of polymer chains under drawing (Fourné 1999).

After passing through the air gap, the fluid filaments enter the aqueous bath where the coagulation of cellulose takes place. The solidification of the thread is

a crucial step in the fiber formation as it involves irreversible structural crystallization in the material which directly affect the mechanical properties of the spun fibers. The precipitation of dissolved cellulose in IL solutions follows the principles of phase separation in polymer solutions. Water, being a polar liquid and miscible with ILs initiates the removal of the solvent from the filaments via an exchange process of solvent against non-solvent (Fink, Weigel et al. 2001). The mechanism of coagulation of cellulose dissolved in IL has not been thoroughly investigated yet but is believed to follow the same solidification process as the NMMO-Lyocell method since the same type of non-derivatizing solvent is employed (Hauru, Hummel et al. 2015). When the fluid filament enters the aqueous coagulation bath, the desolvation of the cellulose molecules and the reformation of the cellulose network takes place, resulting in the formation of a fribrillar cellulose II crystal structure (Fink, Weigel et al. 2001, Gavillon, Budtova 2007, Biganska, Navard 2005). This phase separation process is reported to occur very fast, about 1 – 2 s for a complete coagulation of a 50 µm fiber, preventing the relaxation in chain orientation (Mortimer, Peguy 1996a). The phase separation step, which seems to follow spinodal decomposition, leads to the formation of a rigid layer at the surface of the filament surrounding the fluid core (Biganska, Navard 2005, Eckelt, Eich et al. 2009). The solid-liquid phase boundary moves inwards as the filament travels within the aqueous bath, causing a continuous decrease of the fluid core diameter. Cellulose is fully solidified in the bath and solid filaments are collected at the exit of the bath (Ziabicki 1976, Paul 1968).

3.5.2 Spinning instabilities

The spinnability of a viscoelastic fluid, or its ability to receive irreversible deformation when subjected to uniaxial stress, is an essential aspect to investigate to achieve stable fiber spinning. According to Ziabicki, “a fluid is spinnable under given deformation condition if steady-state, continuous elongation of the fluid jet proceeds without a break of any kind”. The hydrodynamic instability of the extruded jet in the air gap results in low stability of the process (Ziabicki 1976). Four different instabilities or breaches of fluid threads during filament spinning have been described in the literature.

3.5.2.1 Cohesive fracture

Cohesive fracture highly depends on the deformation conditions and the viscoelastic properties of the material. It is observed when the tensile stress in the viscoelastic fluid thread exceeds a critical tensile strength p*, which is proportional to the square-root of the product of the Young’s modulus E and the critical elastic energy per unit volume or resilience K, as reported in Equation 3.

$$p^* = \sqrt{2KE} \tag{3}$$

The decrease of the filament diameter leads to an increase of the tensile stress, which may induce the failure of the filament. The maximum fiber length, L_{max}, can be determined from Equation 4.

$$L_{max} = \ln \frac{\sqrt{2KE}}{3\eta V_0 \xi} \quad (4)$$

where η is the dynamic viscosity, V_o the extrusion velocity and ξ the elongation of the fiber, which is described in Equation 5.

$$\xi = \frac{F}{3\eta\pi R_0^2 V_0} \quad (5)$$

where F is the force applied to the fibers and R_o the original fiber radius.

To avoid cohesive breaches, the product $V_o\eta$ should be reduced or the godet should not work on a constant speed but on a constant force.

3.5.2.2 Melt fracture

Melt fracture, also named elastic turbulence is characterized by an irregular outflow associated with the viscoelastic flow of the material through the spinneret capillary. A smooth and continuous fluid thread is formed at lower shear rate but becomes rough and irregular when increasing the shear rate, resulting in the failure of the filament once the critical shear rate is surpassed. A similar phenomenon is observed at constant shear rate when reducing the extrusion temperature. The viscoelastic properties of the material and its deformation history, spinning temperature and, the length of the spinneret capillary or transit time (average time of residence of the fluid within the channel) and the shape of its inlet strongly influence the extent of this instability (Ziabicki 1976).

3.5.2.3 Capillary fracture

Capillary waves are described by the spontaneous formation of asymmetrical distortions of the fluid surface, associated with surface tension. The thread breaks into drops when the amplitude of the capillary waves reaches the radius of the undistorted fluid. This break is typical for dry-spinning. The maximum possible fiber length, L_{max}, can be determined from Equation 6.

$$L_{max} = \frac{2}{\xi}\left[\ln \frac{R_0}{\delta_0} - \frac{\sigma_s}{3\eta\xi V_0 R_0}\right] \quad (6)$$

where σ_s is the surface tension and δ_o the initial amplitude disturbance defined by the equipment and spinning parameters.

L_{max} is favoured by a reduction of the relative strength $\sigma_s/3\eta$ of the fluid or by modifying the spinning parameters such as spinneret diameter or extrusion velocity (Wirth 2011).

3.5.2.4 Telescopic fracture

The last type of fracture, mainly observed in wet spinning, is called telescopic breach. This phenomenon occurs at the beginning of the coagulation bath and shortly after the spinneret due to the liquid core-coagulated skin structure of the filament. The coagulated material absorbs traction forces by elastic tension until it exceeds the failure stress. The coagulated skin breaks, and a telescope-like displacement of the solid fiber skin and the liquid fiber core is generated (Ziabicki 1976, Paul 1968).

3.5.3 Structural and mechanical properties of spun fibers

The characterization of the produced fibers is an essential part of the production process from a quality control aspect as well as for the optimization of the process. The physical and mechanical properties of spun fibers are tightly connected to the process parameters and tension applied along the line. Normed test methods with specified conditions and evaluation procedures are necessary to obtain comparable and reproducible results. Different organizations providing international norms and rules are established. International Standardisation Organisation (ISO), Commission Européenne de Normalisation (CEN) and Bureau International pour Standardisation des Fibres Artificielles (BISFA) are three of them (Fourné 1999, BISFA 2004).

3.5.3.1 Orientation of cellulose chain

The orientation of the cellulose chains occurring during the different steps of the spinning process is a fundamental characteristic to investigate as it strongly affects the mechanical properties of the spun fibers. It can be assessed through the determination of the birefringence (Δn) of the resulting fibers. A molecularly ordered material demonstrates birefringent characteristic when the refraction of light is dependent of the intrinsic orientation of the material. The birefringence can be defined as the difference between the index of parallel refraction and perpendicular refraction to the fiber axis. The total orientation factor (f_t) is determined by dividing the birefringence by the maximum birefringence of cellulose 0.062, which was calculated through extrapolation when plotting the birefringence vs. the fiber compliance (Adusumalli, Keckes et al. 2009, Sixta, Michud et al. 2015). A factor of 1 means that all of cellulose molecules are aligned parallel to the fiber axis, $f_t = 0$ corresponds to random dispersion and $f_t = -1$ to transverse orientation (Golzar 2004, Röder, Moosbauer et al. 2009).

3.5.3.2 Fiber fineness

The fiber fineness is defined by the linear density or titer. For textile application, the Tex system is employed. Tex is defined as the mass in grams per 1 000 meters of fiber. The titer of a fiber can be determined using the vibration method. Single fibers are set in vibration at their natural frequency. The linear density is then obtained from the resonance frequency, the length of the vibrating section of the fiber and the tensioning weigth placed at the edge of the fiber (Fourné

1999, BISFA 2004). A higher stretching of the fluid filament in the air gap results in thinner fibers. Standard man-made cellulosic textile staple fibers have a titer of 1.2 – 1.7 dtex.

3.5.3.3 Mechanical properties

The tenacity, elongation at break and the elastic modulus of fibers are assessed by tensile tests. These mechanical properties give important information on the strength, extension ability and stiffness of a fiber. The tenacity-elongation curve exhibits the deformation behavior of a fiber under a certain stress load. Two regions are distinguished: the first linear part corresponds to the elastic region and the second one to the plastic region in which the chains start to be stretched and get permanently deformed until the network breaks. Greater degree of alignment results in higher tenacity and lower elongation, due to the tight cellulose network which prevents the cellulose molecules to slide over one another. Larger elastic modulus, which is calculated from the slope of the elastic region, is correlated to a higher resistance of the fiber against deformation (Fourné 1999, Gordon Cook 1984).

3.5.4 Process parameters

The variation of the spinning process parameters enables the optimization and development of a stable spinning which is required to identify the so called spinning window. The mechanical properties of the produced fibers are closely related to the process conditions. The process parameters such as draw ratio, extrusion velocity, spinneret geometry, air gap and coagulation bath conditions all affect significantly the formation of the molecular structure of the fibers by modifying the flows and stresses present in the different shaping zones.

3.5.4.1 Draw ratio

The molecular orientation of the cellulose chains is the key structural characteristic affecting the mechanical properties of the resulting fibers. The birefringence of the dried fibers is strongly connected to the draw ratio applied to the fluid filament in the air gap. Mortimer reported that a small draw was sufficient to highly orient the semi-crystalline structure of NMMO-Lyocell fibers. According to this study, the birefringence is developed rapidly at low draws and stabilizes at a draw of about 5. At this relatively low draw, the cellulose chain might have already reached their full extension and, hence, their maximum achievable orientation. Furthermore, the reduction of the die swell at the exit of the spinneret was also reported at higher draws due to the higher take-up force. A gain in birefringence results in greater Young's modulus and tenacity, and a diminution in the elongation at break (Mortimer, Peguy et al. 1996, Mortimer, Peguy 1996a). Cai et al. also reported a similar increase in mechanical properties for IL-based fibers with an increase of the draw ratio (Cai, Zhang et al. 2010).

3.5.4.2 Spinneret nozzle diameter

At constant extrusion velocity, the spinneret geometry has an impact on the molecular orientation of the polymer chains in the air gap. Evidently, the spinneret diameter plays a significant role in the thickness of the fluid filament which is larger with the use of bigger nozzle spinneret. Thicker filaments undergo slower cooling due to the reduction of the surface area to volume ratio. This slower cooling decelerates the increase in viscosity and causes a diminution in stress within the filament, affecting the extension of the chains in the air gap. Longer draw lengths are thus required with larger nozzle diameters to attain an orientation level equivalent to the one reached with lower throughput. Mortimer also observed greater die swell with larger filaments (Mortimer, Peguy et al. 1996, Mortimer, Peguy 1996a, Mortimer, Peguy 1996b).

3.5.4.3 Extrusion velocity

At constant spinneret diameter, the augmentation of the extrusion velocity corresponds to an increase of the throughput. As explained previously, a longer draw length is consequently required to obtain an equivalent molecular orientation due to the slower cooling of the filament. Jiang et al. reported superior mechanical properties of IL-based fibers with the increase of the extrusion velocity due to the augmentation in stress in the spun filament whereas Mortimer et al. detected no significant effect of the speed line on the orientation and mechanical properties of Lyocell fibers (Jiang, Yuan et al. 2012, Mortimer, Peguy et al. 1996).

3.5.4.4 Air gap

The air gap length and conditioning have a significant influence on the physical properties of the spun fibers as most of the chain orientation occurs between the spinneret exit and the entrance of the coagulation bath. Long air gaps permit the velocity of the material and the related stress within the filament to reach their final level, leading to equivalent birefringence independently from the spinneret size. However, with larger spinneret, the reduction of the air gap results in lower orientation at the entrance of the bath as the filament has less time to cool down and the stress has shorter time to increase. Cold and dry air gaps favor the cooling of the filament, which results in higher viscosity and stress within the filament. Shorter draw length are hence sufficient with cooled and dried air to reach the targeted birefringence. Mortimer also observed the reduction of the die swell with short air gap due to the forced acceleration of the material to the coagulation bath. The use of cold and dry air gap resulted in the decrease of the die swell as well. The properties of the final fibers are closely related to the chain orientation developed in the air gap and thus follow the same trend as the birefringence.(Mortimer, Peguy 1996b).

3.5.4.5 Coagulation bath

The temperature and solvent content of the coagulation bath affect the solidification of the thread due to their influence on the diffusion rate of the solvent

from the filament to the bath. Song et al. demonstrated that the diffusion rate of [AMIM]Cl increases with the rise of the precipitation bath temperature due to the accelerated movements of the molecules and the formation of pores at the skin surface. An increase of the concentration of IL in the bath reduces the solidification rate of the filament as the coefficient of diffusion is diminished. A maximum diffusion rate was achieved at a concentration of 5% of [AMIM]Cl in the bath (Song, Cheng et al. 2011).

3.5.4.6 Solute characteristics

The intrinsic characteristics and the concentration of the dissolved cellulose influence significantly the final properties of the fibers. Higher DP or concentration of cellulose favor the formation of a more cohesive network which results in greater mechanical properties (Olsson, Westman 2013b, Hong, Ku et al. 2013, Kim, Pak et al. 2005, Mülleder, Schrempf et al. 1998). On the other hand, higher concentration leads to slower precipitation of cellulose as the diffusion rate of the solvent into the bath is reduced. The lower solvent content in the filament diminishes the solvent concentration gradient between the material and the bath, leading to a decrease in the diffusion coefficient (Song, Cheng et al. 2011).

4. Experimental

4.1 Materials

4.1.1 Raw materials

Eucalyptus (*Eucalyptus urugrandis*) prehydrolysis kraft pulp (E-PHK) from Bahia Speciality Copener with intrinsic viscosities, η, of 424 ml/g was employed for the experiments in Papers I, II and III. Birch (*Betula pendula*) prehydrolysis kraft pulp (B-PHK) supplied by Stora Enso Enocell pulp mill with an intrinsic viscosity of 476 ml/g was used for the experimental part in Papers II and IV. Cotton linters from Milouban M.C.P Ltd and spruce sulfite pulp supplied by Borregaard with intrinsic viscosities of 729 (cotton linters CL1) and 524 (cotton linters CL2), 577 (spruce S1-S) and 1521 (spruce S2-S) ml/g were utilized for the experiments in Paper III. In this paper, the preparation of blends of similar intrinsic viscosity but various MMD required the degradation of CL1 and S1-S in sodium hydroxide. The degraded pulps are denoted CL1-420, CL1-415, CL1-318, S1-S218, S1-S192, S1-S174, the value corresponding to the resulting intrinsic viscosity. Table 4.1 summarizes the characteristics of the original and degraded pulps used in the different studies. The original pulps were delivered in sheet form and ground by means of a Wiley mill with a mesh size of 0.5 mm.

Table 4.1. Intrinsic characteristics of original and degraded pulps.

	η	Cellulose %	Hemi-cellulose %	M_n	M_w	PDI	DP<100	DP>2000
	ml/g			kDa	kDa	-	%	%
E-PHK	424	94.6	5.3	79.8	268.7	3.4	3.0	27.1
B-PHK	476	95.8	2.6	65.9	269.3	4.1	4.6	25.5
CL1	729	95.7	-	159.3	350.4	2.2	0.3	37.5
CL2	524	95.0	-	130.3	259.6	2.0	0.3	25.7
S1-S	577	96.9	2.2	54.7	321.4	5.9	5.7	28.2
S2-S	1521	92.9	3.6	109.4	948.5	8.7	3.5	64.4
CL1-318	318	-	-	70.8	157.7	2.2	2.6	9.6
CL1-415	415	-	-	101.0	204.0	2.0	1.0	17.0

CL1-420	420	-	-	104.6	209.9	2.0	0.8	17.9
S1-S174	174	-	-	37.7	100.1	2.7	8.3	3.4
S1-S192	192	-	-	33.8	80.7	2.4	10.1	1.4
S1-S218	218	-	-	32.3	75.3	2.3	11.3	1.1

4.1.2 Ionic liquids

1-Ethyl-3-methyl imidazolium acetate with a purity superior to 95% was purchased from BASF (Germany) and employed without any further purification for the experiments in paper I. A water content of 0.13% was determined via Karl-Fisher titration. [EMIM]OAc is a RTIL, as shown in Figure 4.1.

1,5-Diazabicyclo[4.3.0]non-5-enium acetate was prepared at the University of Helsinki in Paper II and in our laboratory in papers III and IV by neutralization of 1,5-diazabicyclo[4.3.0]non-5-ene, DBN, (99%, Fluorochem, UK) with acetic acid (glacial, 100%, Merck, Germany). Both components were utilized as received, acetic acid was gradually added under external cooling due to the exothermic nature of the reaction until reaching an equimolar ratio. The solution was stirred for 1 h at 80 °C after complete addition of the required amount of acetic acid. [DBNH]OAc, depicted in Figure 4.1, solidifies at room temperature and shows a melting temperature of 60 °C.

Figure 4.1. [EMIM]OAc (left) and [DBNH]OAc (right) at room temperature.

Purity and thermal stability of [EMIM]OAc and [DBNH]OAc have been investigated via nuclear magnetique resonance (NMR) in DMSO-d_6 and, thermogravimetric analysis (TGA) and differential scanning calorimetry (DSC), respectively. Figures 4.2 and 4.3 exhibit the ^{1}H and ^{13}C NMR spectra of [EMIM]OAc and [DBNH]OAc, which were collected using Varian 300 MHz Unity spectrometer and processed with MestreLab Research, MestReC 23 software. The purity of the ILs were assessed by affiliating each peak of the spectra to the corresponding proton or carbon in the chemical structure. The spectra show clear peaks and no extra peak from degradation products were observed (Parviainen, Wahlström et al. 2015).

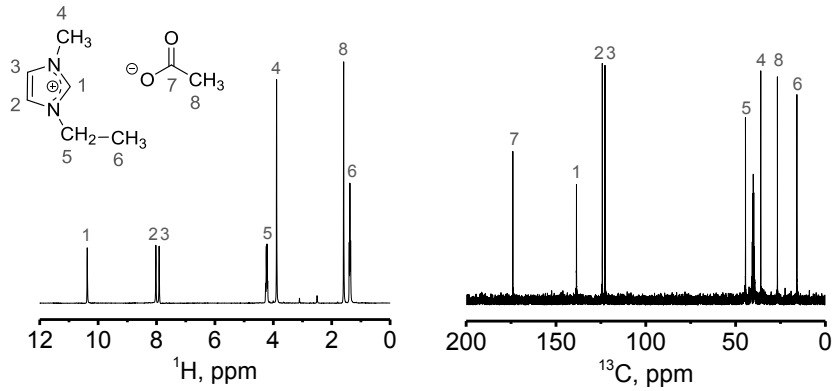

Figure 4.2. ^{1}H (left) and ^{13}C (right) NMR spectra of [EMIM]OAc.

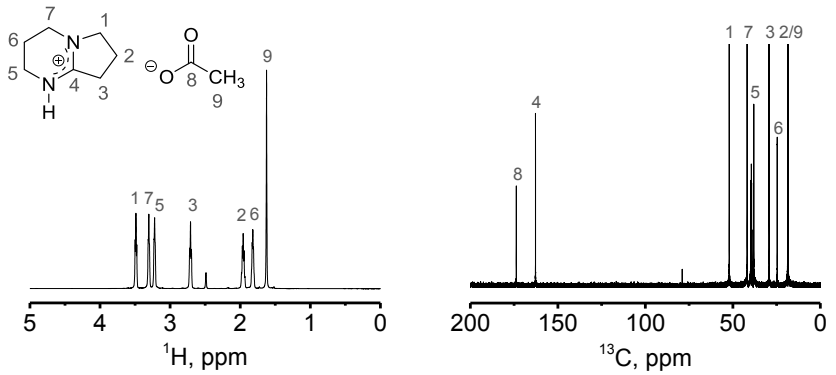

Figure 4.3. ^{1}H (left) and ^{13}C (right) NMR spectra of [DBNH]OAc.

Figure 4.4 depicts the [EMIM]OAc and [DBNH]OAc TGA thermal curves, which indicate the weight loss (%) as a function of temperature (°C). We can notice that the onset temperature, which denotes the temperature at which the weight loss begins, of [DBNH]OAc is lower than the onset temperature of [EMIM]OAc. This earlier weight loss might be explained by the distillable characteristic of [DBNH]OAc, particularly the potential evaporation of the DBN component, and does not necessarily correspond to the degradation of the IL.

Figure 4.5 shows the [EMIM]OAc and [DBNH]OAc DSC curves, which display the heat flow (mW) as a function of temperature (°C). The onset of melting of [DBNH]OAc and the endothermic peak, corresponding to complete melting, are observed.

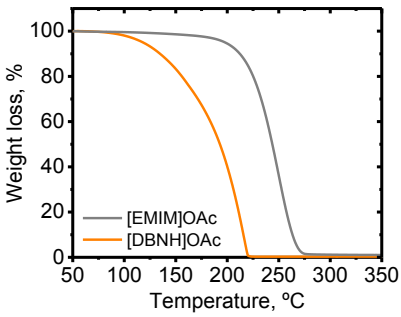

Figure 4.4. TGA curves of [DBNH]OAc and [EMIM]OAc showing the weight loss (%) as a function of temperature (°C).

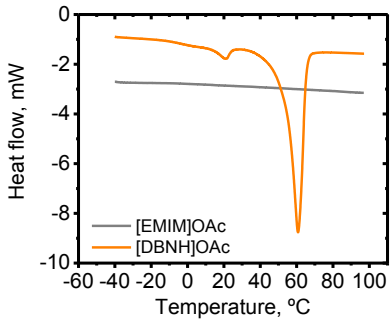

Figure 4.5. DSC curves of [DBNH]OAc and [EMIM]OAc denoting the heat flow (mW) as a function of temperature (°C).

NMR analysis showed that heating [DBNH]OAc with water undergoes the formation of (aminopropyl)-2-pyrrolidonium acetate ([APPH]OAc) as described in Figure 4.6 (Parviainen, Wahlström et al. 2015).

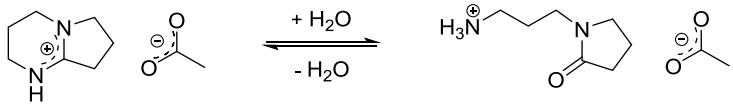

Figure 4.6. Hydrolysis of [DBNH]OAc to [APPH]OAc (Parviainen, Wahlström et al. 2015).

The shear viscosity of [EMIM]OAc and [DBNH]OAc is represented as a function of temperature in Figure 4.7. They show comparable viscosity behavior from a temperature of 60 °C, which corresponds to the melting point of [DBNH]OAc.

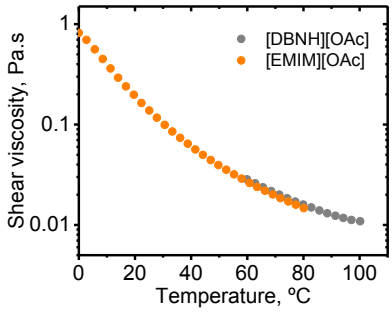

Figure 4.7. Shear viscosity (Pa.s) of [DBNH]OAc and [EMIM]OAc as a function of temperature (°C).

4.2 Equipment

4.2.1 Preparation of cellulose/ionic liquid solution

The pulps were dissolved in IL by means of a vertical kneader, shown in Figure 4.8. The temperature, pressure and rotation per minute of the system were set at 95 °C, 55 mbar and 48 rpm for the experiments described in paper I and 80 °C, 100 mbar and 10 rpm in papers II, III and IV. A dissolution time of 60 min was sufficient for the complete dissolution of the cellulose pulps listed in paragraph 4.1.1. The state of the dissolution was confirmed by means of an optical microscope after 60 min of stirring. In papers II, III and IV, the resulting polymer solutions were filtered via a hydraulic pressure filtration unit (1 – 2 MPa, metal filter fleece, 5 – 6 µm absolute fineness, Gebr. Kufferath AG, Germany), depicted in Figure 4.9, to remove any impurities or undissolved particles, and assure constant solution quality during spinning. The loading of the solution into the spinning cylinder was facilitated by shaping the solutions according to the dimension of the cylinder and letting them solidify for 1 – 2 days after preparation. A 10 weight-% cellulose/[EMIM]OAc solution was prepared in paper I and 13 wt-% cellulose/[DBNH]OAc solutions were prepared in papers II, III and IV.

Figure 4.8. Vertical kneader for cellulose dissolution.

Figure 4.9. Hydraulic pressure filtration unit.

4.2.2 Rheological characterization of cellulose/ionic liquid solution

4.2.2.1 Oscillatory shear rheology

The viscoelastic properties of the polymer solutions were evaluated via oscillatory shear rheology by means of an Anton Paar MCR 300 with a plate and plate geometry (25 mm diameter, 1 mm gap size), as shown in Figure 4.10. First, dynamic strain sweep tests were conducted to define the linear viscoelastic domain and select an adequate strain for the subsequent frequency sweep tests. Strains of 1% for [EMIM]OAc solutions and 0.5% for [DBNH]OAc solutions were chosen. An angular frequency range of 0.01 – 100 s^{-1} at temperatures from 70 to 90 ^{o}C was applied during frequency sweep. Complex viscosity, η^*, as well as the dynamic moduli, G' and G", were recorded. As suggested by Sammons et al., complex viscosity data were fitted to the three-parameter Cross viscosity model (Equation 7) to determine the zero-shear viscosity, η_0 (Sammons, Collier et al. 2008b). The Cox-Merz rule is here assumed to be valid (Lu, Cheng et al. 2012).

$$\eta = \frac{\eta_0}{(1+(\lambda\dot{\gamma})^{1-n})} \qquad (7)$$

where λ is a time constant and n the power-law exponent.

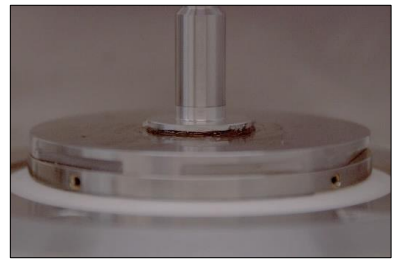

Figure 4.10. Anton Paar MCR 300 with plate-plate geometry. Above: sample loaded between the two plates.

4.2.2.2 Capillary break-up extensional rheology

The extensional rheological analyses carried out in paper I were performed with a Thermo Fisher capillary break-up extensional rheometer (CaBER) depicted in Figure 4.11. Plates of 6 mm were employed and the step-stretch was defined by an initial and final aspect ratio of 0.66 and 3.00, corresponding to an initial and final separation of the plates of 2 and 9 mm, respectively. An equilibration time of 2 min was set between the loading of the sample and the start of the measurement in order to delete the effects deriving from shear during loading. Potential moisture take-up was prevented during the tests by purging a dry-air flow of 1.5 ml/min through the measurement cell.

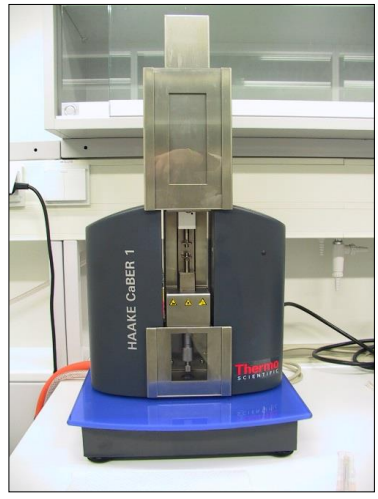

Figure 4.11. Capillary break-up extensional rheometer (CaBER).

4.2.2.3 Elongation viscosity via radial force measurement

The determination of the elongational viscosity in Paper IV was conducted via the measurement of the total force acting on the bundle of filaments at the exit of the coagulation bath as a function of the reciprocal air gap length. The total force (F_{tot}) after the bath is considered to be composed of the hydrodynamical (F_{hydr}) and rheological forces (F_{rheo}) given by Equation 8 (Boerstoel 1998).

$$F_{tot} = F_{rheo} + F_{hydr} \tag{8}$$

The filament velocity is defined by an exponential profile (Equation 9) when only the external and rheological forces are considered in the force balance acting on the fluid filament in the air gap (Boerstoel 1998).

$$v_1 = v_0 \, exp\left(\frac{F_{rheo} l}{Q\eta_e}\right) \tag{9}$$

where Q is the throughput outflow, η_e the elongational viscosity, v_0 the extrusion velocity and v_1 the take-up velocity equal to the velocity of the filament at the surface of the bath.

By combining Equations 8 and 9, the elongational viscosity is extracted from the slope of the plot representing the total force versus the reciprocal air gap length, l, as shown in Equation 10.

$$F_{tot} = \frac{Q\eta_e}{l} \ln\left(\frac{v_1}{v_0}\right) + F_{hydr} \tag{10}$$

F_{tot} is measured by means of a strain gauge-based force sensor placed at the exit of the coagulation bath, as illustrated in Figure 4.12. The measuring principle is based on the evaluation of the forces acting radially into the sensor, as described in Figure 4.13. The load transmission is effected through the pulley which is mounted onto the sensor's bearing journal.

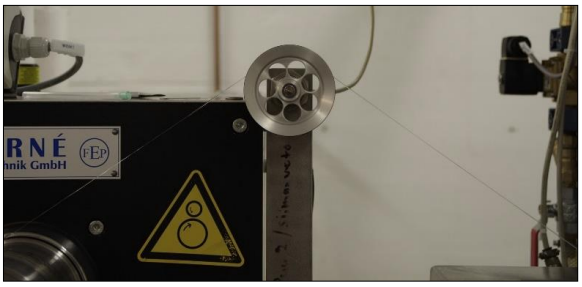

Figure 4.12. Radial force sensor at the exit of the coagulation bath.

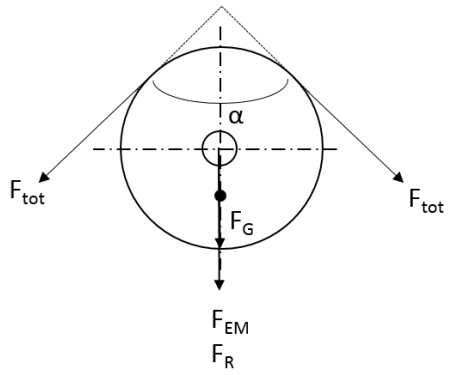

Figure 4.13. Forces acting on the sensor's bearing axis.

where
α is the wrap angle at reversing angle

$\vec{F}_{tot}$ is the tension force

$\vec{F}_{EM}$ is the effective measurement force applied to the sensor

$\vec{F}_{R}$ is the force resulting from tension force and wrap angle

$\vec{F}_{G}$ is the weight of the reversing roller due to the force of gravity

The resulting force F_R is calculated by subtracting the weight F_G of the reversing roller to the effective measurement force F_{EM} according to Equation 11.

$$F_R = F_{EM} - F_G \tag{11}$$

The tension force F_{tot} is calculated on the basis of the resulting force F_R and the wrap angle α, according to Equations 12 and 13.

$$\cos\frac{\alpha}{2} = \frac{|\vec{F}_R|}{2|\vec{F}_{tot}|} \tag{12}$$

$$F_{tot} = \frac{F_R}{2\cos\frac{\alpha}{2}} \tag{13}$$

4.2.3 Spinning of cellulose/ionic liquid solution

Cellulosic multi-filaments were spun with a customized laboratory dry-jet wet spinning unit supplied by Fourné Polymertechnik, Germany, depicted in Figure 4.14.

Figure 4.14. Dry-jet wet spinning unit at Aalto University.

It consists of a piston/extrusion unit, coagulation bath, washing bath, drying channel, 4 godet couples and a winder, as represented in Figure 4.15. For practical issues, fibers were collected at the first godet, the washing and the drying steps were conducted offline. Fibers were washed in water at 70 ºC for 1h and dried at room temperature tension free. The characteristics of the spinning unit are listed below.

Filing capacity	500 ml
Extrusion velocity range	0.4 – 5 ml/min
Godet velocity range	5 – 100 m/min
Winder velocity range	5 – 70 m/min

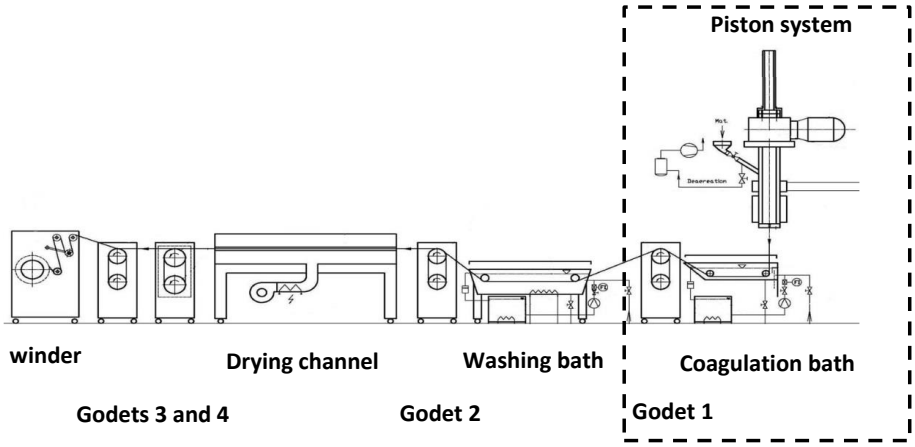

Figure 4.15. Schematic representation of the dry-jet wet spinning line.

Spinnerets with different diameters were employed during the experiments. They are summarized in Table 4.2.

Table 4.2. List of the spinnerets employed in the different studies.

Spinneret	Publication
36 x 100 µm, L/D* 0.2	II, III, IV
36 x 150 µm, L/D 0.2	IV
36 x 200 µm, L/D 0.2	IV

*length/diameter ratio of the spin capillary

4.2.4 Characterization of ionic liquid-based fibers

4.2.4.1 Tensile measurement

The linear density, tenacity and elongation at break of the resulting fibers were assessed by two Lenzing Instrument devices, vibroskop and vibrodyn 400 (Figure 4.16), at 23 °C and 50% humidity. The fibers were conditioned for 24h prior to the tests. The tensile measurements comprise a gauge length of 20 mm, a pretension of 5.9 ± 1.2 mN/tex, and a speed of 20 mm/min according to DIN 53816. The elastic modulus or Young's modulus of the spun fibers was calculated using a matlab program determining the slope of the entire elastic region of the stress-strain curves obtained from the tensile tests according to ASTM Standard D2256/D2256.

Figure 4.16. Lenzing instrument vibroskop (left) and vibrodyn (right).

4.2.4.2 Fiber diameter

The diameter of the fibers was calculated from the titer using the cellulose density value of 1.5 g/cm³ according to equation 14.

$$d = 2 \times 10^6 \sqrt{\frac{t}{10^{10}\rho\pi}} \qquad (14)$$

where

d is the diameter in µm

t is the titer in dtex

ρ is the linear density in g/cm³

4.2.4.3 Birefringence measurement

A Zeiss Axio Scope polarized microscope, equipped with a 5λ Berek compensator, was adopted to evaluate the birefringence and total orientation of the fibers (Figure 4.17). Light when entering a birefringent material is refracted into two linear polarized lights: ordinary rays, following the law of refraction, and extraordinary rays, as shown in Figure 4.18. The optical axis and the direction of the incident light determine the vibration direction of the two rays in an optically uniaxial material. The section containing both rays is named the principal section. The ordinary rays ocsillate vertically through the principal section while the extraordinary ones oscillate within the principal section. They travel the anisotropic material at different velocities and have different refractive indices. The birefringence, Δn, of the fibers was obtained by dividing the retardation of the polarized light, Γ_λ, by the thickness of the fiber, d. The retardation was assessed from the tilting angles obtained by tilting the compensator plate until the phase difference in the material was completely compensated. The calculation of the birefringence and light retardation are described by equations 15 and 16. The total orientation was determined by dividing Δn by the maximum birefringence of cellulose 0.062 (Adusumalli, Keckes et al. 2009, Gindl, Reifferscheid et al. 2008).

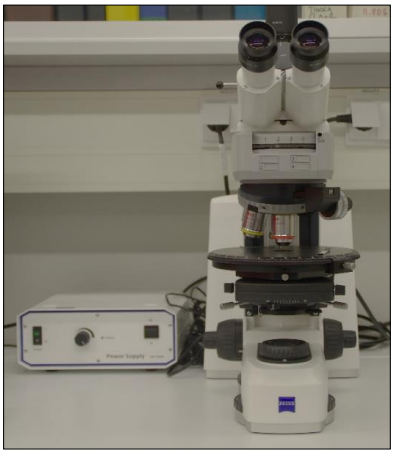

Figure 4.17. Zeiss Axio Scope polarized microscope equipped with a 5λ Berek compensator.

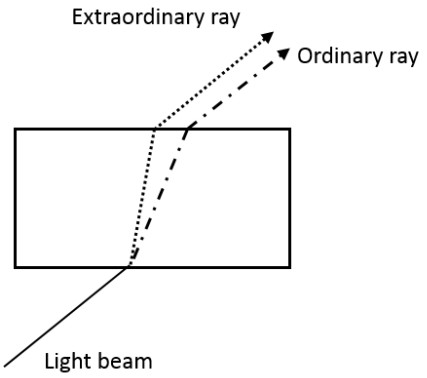

Figure 4.18. Vibration direction of ordinary and extraordinary rays of an optically uniaxial material.

$$\Delta n = \frac{\Gamma_\lambda}{d} \qquad (15)$$

where

Γ_λ is the retardation of the polarized light in nm = 10^{-6} at wavelength λ

d is the thickness of the fiber in nm

$$\Gamma_\lambda = d_c . n_0 \left(\sqrt{1 - \frac{sin^2\, i}{n_e^2}} - \sqrt{1 - \frac{sin^2\, i}{n_0^2}} \right) \quad (16)$$

where
d_c is the thickness of the compensator plate (1.52 nm)

n_o is the refractive index of the ordinary wave of the compensator plate (1.37859)

n_e is the refractive index of the extraordinary wave of the compensator plate (1.39043)

i is the angle of the tilt of the plane of the plate against the zero position = position vertical to the propagation of the light

5. Results and discussion

5.1 Solubility and thermal stability of cellulose in ionic liquid

5.1.1 Solubility of cellulose in ionic liquid

B-PHK and E-PHK pulps, shredded to fine particles, showed very good solubility in both [EMIM]OAc and [DBNH]OAc ILs without any additional pre-treatments. The target intrinsic viscosity of the dissolved cellulose was 450 ml/g corresponding to a DP 1047, which is in accordance with the DP of NMMO-based Lyocell pulps. The vertical kneader system allowed for fast dissolution under constant shearing and high vacuum at mild temperature. Based on the target DP, a dissolution time between 45 and 75 min (depending on the cellulose concentration and amount to dissolve), a dissolution temperature of 80 °C, a shearing rate of 10 rpm and a vacuum of 100 mbar were set as optimum conditions for cellulose dissolution. The equilibrium pulp moisture was the only water present in solution during dissolution. Solutions with a concentration up to 17 wt-% of cellulose could be prepared. However, concentrations exceeding 14 wt-% imply higher solution viscosity and thus more difficulties for handling and processing.

The water content in the starting cellulose/IL suspension appeared to be of great importance for the successful dissolution of cellulose. The influence of water in [DBNH]OAc on the dissolution of B-PHK air-dried pulp was investigated and resulted in the identification of a water content limit of 5.5 wt-% in solution, including the equilibrium pulp moisture content (unpublished data). Figure 5.1 shows the optical microscope images of the dissolution state of 13 wt-% B-PHK solutions containing 5.5, 8.4 and 10.5 wt-% of water after 60 min of kneading.

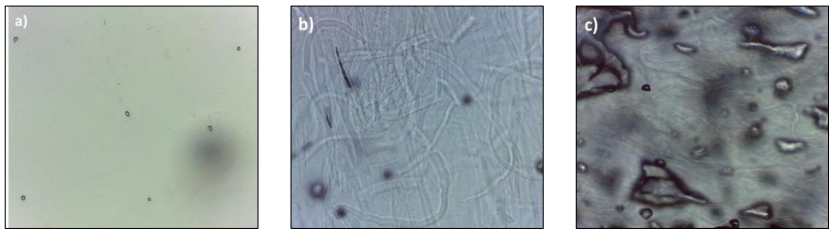

Figure 5.1. Optical microscope images of 13 wt-% B-PHK/[DBNH]OAc solution containing a) 5.5 wt-%, b) 8.4 wt-%, c) 10.5 wt-% of water, including the equilibrium pulp moisture content of typically 6 wt-% on pulp.

5.1.2 Thermal stability of cellulose in ionic liquid

Cellulose demonstrated thermal instability when processed at a temperature higher than 85 °C in [EMIM]OAc. A significant reduction in cellulose DP of 25.2% was observed at a dissolution temperature of 95 °C with [EMIM]OAc for 1h. A decrease of 10 °C of the dissolution temperature reduced the extent of degradation to about 10% (Paper I). The cellulose degradation occurring in [EMIM]OAc is depicted in Figure 5.2, which exhibits the average number of chain scission per chain unit and the cellulose DP before and after dissolution at 95 °C and as a function of the storage time at 60, 90 and 110 °C. The severe degradation occurring during the dissolution step at 95 °C is represented by the grey area. The effect of the stabilizer propyl gallate is observed through the substantial reduction of the number of chain scission at 0h.

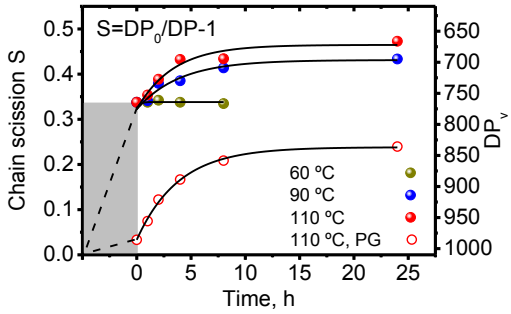

Figure 5.2. Scission per cellulose chain and DP of cellulose dissolved in [EMIM]OAc at 95 °C and degraded at 60, 90 and 110 °C upon storage time. The grey area represents the chain scission occurring during the dissolution step (Paper I).

The selected dissolution conditions of cellulose in [DBNH]OAc (80 °C, 75 min, 10 rpm) prevented serious degradation of cellulose and led to a decrease of the DP of about 6%. Figure 5.3 depicts the molar mass distribution of E-PHK and B-PHK pulps before dissolution and of the precipitated cellulose after dissolution. A small diminution of the share of the long cellulose chains is noticeable, increasing hence the fraction of medium length cellulose chains in the regenerated cellulose (unpublished data).

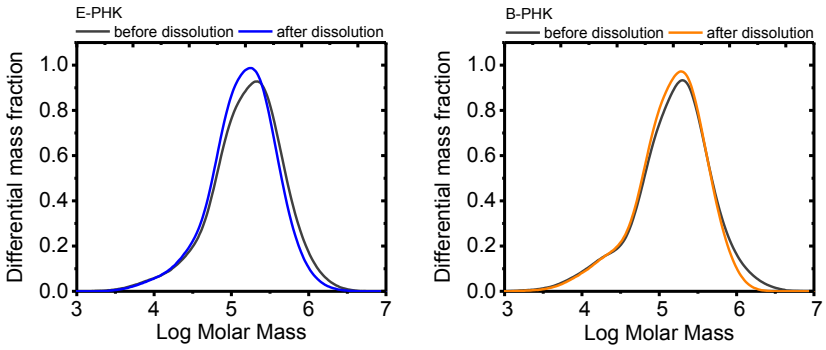

Figure 5.3. Molar mass distribution of E-PHK and B-PHK pulps before and after dissolution in [DBNH]OAc for 75 min at 10 rpm and 80 °C.

5.2 Rheological properties of cellulose/ionic liquid solution

5.2.1 Oscillatory shear rheology

5.2.1.1 Influence of cellulose concentration

The concentration of cellulose has a strong effect on the shear rheological properties of ionic liquid solution. Figure 5.4 depicts the complex viscosity and the storage and loss moduli of 13 and 15 wt-% E-PHK in [DBNH]OAc (unpublished data). The formation of a more entangled and denser cellulose network with higher concentration was observed through the increase of the complex viscosity and the shift of the COP between the loss and storage moduli to lower angular frequency. The COP defines the shear rate at which the elastic behavior of the solution exceeds the viscous behavior. At higher cellulose concentration, the elastic properties predominate due to the more entangled intrinsic structure, the elastic region thus widens and the viscous one narrows. A shear thinning behavior for the complex viscosity was observed with increasing frequencies due to a reduction of the number of entanglements between cellulose chains as they tend to orient. Sammons et al. and Chen et al. reported similar shear behavior with solutions of cellulose dissolved in 1-butyl-3-methylimidazolium chloride ([BMIM]Cl) (Sammons, Collier et al. 2008b, Chen, Zhang et al. 2009).

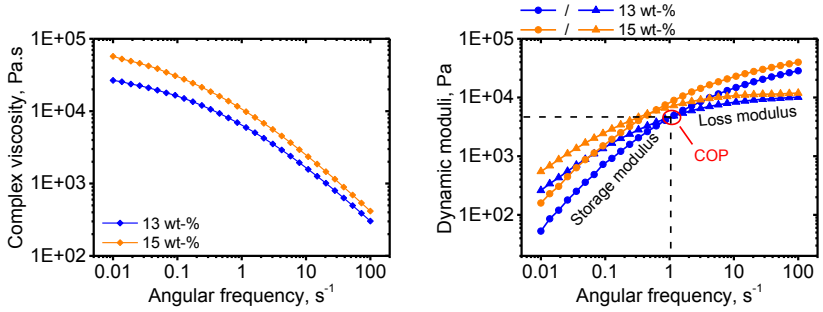

Figure 5.4. Complex viscosity (left) and loss and storage moduli (right) of 13 (blue) and 15 (orange) wt-% E-PHK in [DBNH]OAc at 75 °C.

5.2.1.2 Influence of temperature

The shear properties of the 13 wt-% E-PHK/[DBNH]OAc solution were significantly influenced by the testing temperature. Figure 5.5 illustrates the effect of increasing temperature on the complex viscosity and dynamic moduli of a 13 wt-% solution (unpublished data). At higher temperatures, the interactions between the molecule chains become weaker, the chains get more freedom to move and flowability is improved which results in lower viscosity. For similar reasons, the viscous properties predominate over a larger frequency range, the COP is shifted to a higher angular frequency. However, the modulus value of the COP is not modified as the number of entanglement points does not change. Comparable trends were presented by Sammons et al. and Chen et al. with cellulose/[BMIM]Cl solutions (Chen, Zhang et al. 2009, Sammons, Collier et al. 2008b).

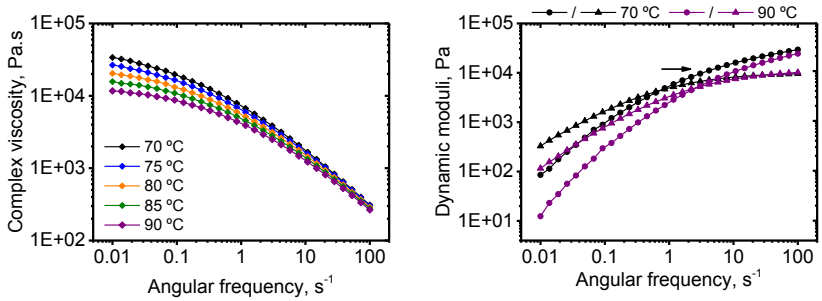

Figure 5.5 Influence of temperature on complex viscosity and dynamic moduli of 13 wt-% E-PHK/[DBNH]OAc solutions.

5.2.1.3 Influence of cellulose molar mass distribution

The MMD of cellulose demonstrated a significant influence on the shear rheology and spinnability of cellulose/[DBNH]OAc solution. Figure 5.6 exhibits the MMD of 6 cellulose blends and E-PHK pulp of comparable intrinsic viscosities (420 ml/g). Table 5.1 lists the blend composition.

Table 5.1. Blend composition.

Blend	Pulp A	Pulp B
1	S2-S, 21.7%	S1-S218, 78.3%
2	S1-S, 75.2%	S1-S174, 24.8%
3	CL1, 2%	CL1-415, 98%
4	CL1-420, 100%	-
5	S2-S, 9.5%	S1-S192, 90.5%
6	CL2, 68.7%	S1-S192, 31.3%

Despite similar intrinsic viscosities, the respective blend-pulp/[DBNH]OAc solutions showed very different viscoelastic properties. Figure 5.7 A) depicts the zero-shear viscosity calculated from the Cross model (Equation 7) as a function of the angular frequency of the COP. As previously mentioned, the increase of the temperature or decrease of the concentration results in lower viscosities and a shift of the COP to higher angular frequency. At comparable temperature, IL solutions with larger share of long cellulose chains show a lower angular frequency of COP and higher zero-shear viscosity due to a strengthened network. The differences in viscoelastic properties are more evident in Figure 5.7 B), demonstrating the dynamic modulus of the COP as a function of the angular frequency of COP. It appears that the presence of longer cellulose chains shifts the COP to higher modulus (paper III).

Shear rheology appears hence to be a suitable method to monitor the MMD of cellulose in solution as the viscoelastic properties is mainly affected by the share of very long molecules, DP>2000. The degradation of cellulose in IL can hence be followed not only by DP and MMD characterization of the precipitated cellulose but also by directly measuring the viscoelastic properties of the IL solution via oscillatory shear measurements. The reduction in the DP of cellulose dissolved in [EMIM]OAc was monitored over time at 60, 90 and 110 °C via shear rheology in Paper I. While no differences in viscoelastic properties were observed at 60 °C, the complex viscosity gradually decreased and the COP was shifted toward higher angular frequency over time at 90 and 110 °C (Figure 5.8), indicating a more liquid-like behavior of the solution due to the reduction of cellulose DP and weaker entanglement network (Paper I).

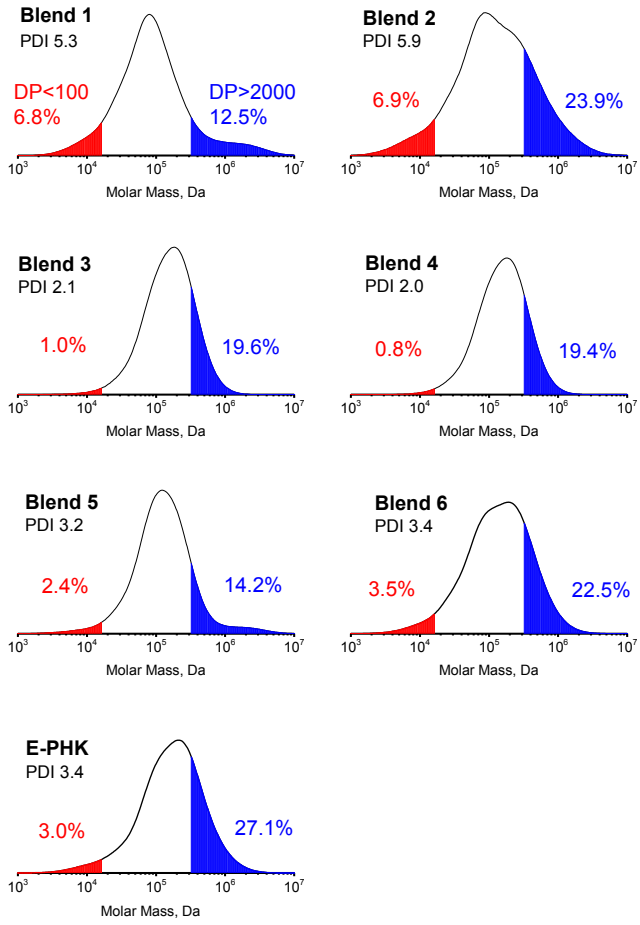

Figure 5.6. Molar mass distribution of cellulose blends and E-PHK pulp (Paper III).

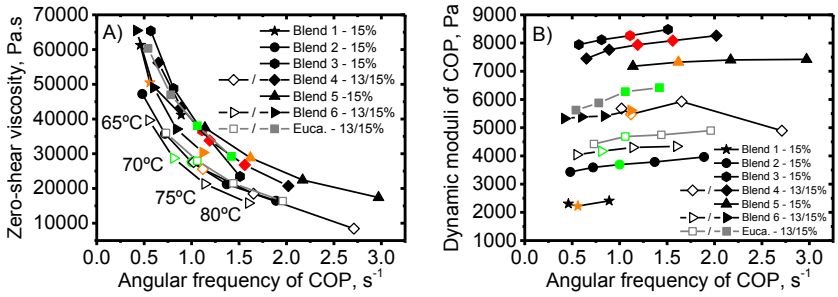

Figure 5.7. A) Zero-shear viscosity and B) dynamic moduli of COP as a function of the angular frequency of COP of cellulose blends and E-PHK pulp in [DBNH]OAc (Paper III). Green dots: successful spinning, orange dots: intermediate spinning, red: unsuccessful spinning.

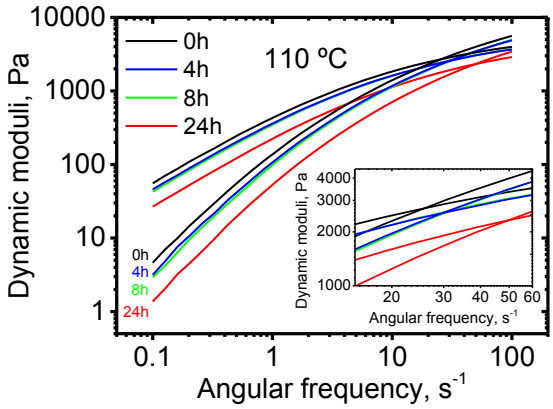

Figure 5.8. Dynamic moduli of 10 wt-% E-PHK/[EMIM]OAc solution stored at 110 °C (measured at 60 °C). The inset shows a zoom on the COP.

5.2.2 Extensional properties of ionic liquid/cellulose solution

5.2.2.1 Capillary break-up extensional rheology (Paper I)

Elongational rheology appeared to be also an appropriate method to examine the potential degradation of cellulose in ILs as the extensional behavior of viscoelastic solutions is related to the chain-chain interactions in solution. The temperature-induced decrease in DP over time of E-PHK pulp dissolved in [EMIM]OAc could be monitored by CaBER. The reduction in DP was observed over time through the faster thinning and thus shorter break-up time of the fluid filament. Figure 5.9 A) illustrates this trend for a solution of 10 wt-% E-PHK pulp dissolved in [EMIM]OAc and stored at 110 °C for 0 to 24h. Figure 5.9 B) exhibits the evolution of the extension rate and apparent extensional viscosity during a measurement of the E-PHK/[EMIM]OAc solution stored at 110 °C for 8h. The three first regimes of the fluid filament thinning are observed. The extension rate, after a significant drop in regime I, slightly increases in regime II followed by a subtential increase in regime III during which the disentanglement and orientation of cellulose occur. The transient extensional viscosity shows a plateau after a drastic increase in regime I. The ultimate elasto-capillary regime characterized by a rise in extensional viscosity (strain hardening) and a plateau of the extension rate as described by Clasen et al. is not observed (Clasen 2010). The missing elasto-capillary regime demonstrates the insensitivity of the CaBER toward high cellulose concentration to detect this last regime required to calculate the elongational relaxation time.

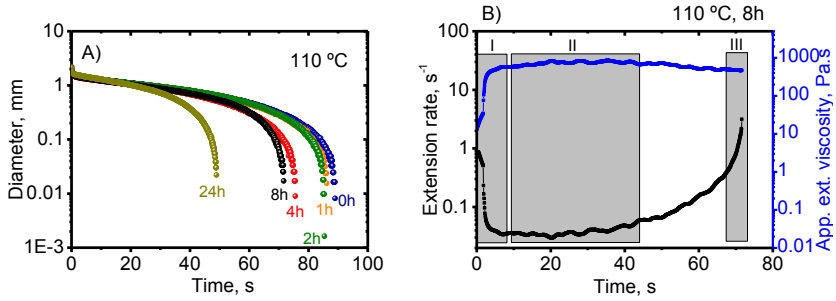

Figure 5.9. A) Evolution of the mid-filament diameter vs. time for E-PHK/[EMIM]OAc 10 wt-% solutions stored at 110 °C at varying retention time. B) Extension rate and apparent extensional viscosity vs. time for the unstabilized E-PHK/[EMIM]OAc solution stored for 8h at 110 °C. (Paper I)

5.2.2.2 Elongational viscosity via force measurement (Paper IV)

Radial force measurement of the filament tow at the exit of the coagulation bath appeared to be an appropriate method for the determination of the elongational viscosity of cellulose/IL solution. The extensional viscosities of 13 wt-% B-PHK/[DBNH]OAc solutions extruded at three different speeds with two different spinneret sizes were assessed. Figure 5.10 presents the force acting on the bundle of the regenerated cellulose filaments exiting the coagulation bath, collected at a draw ratio of 1.5, as a function of the reciprocal air gap length. The elongational viscosities were calculated from the slope according to Equation 10 and are summarized in Table 5.2.

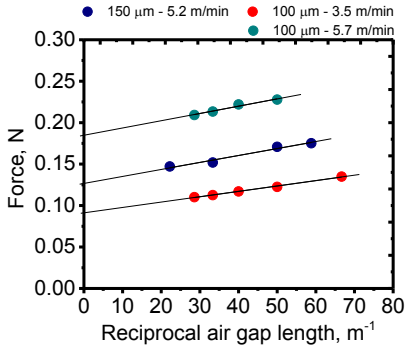

Figure 5.10. Force acting on the filament tow at the exit of the coagulation bath as a function of the reciprocal air gap length for 13 wt-% B-PHK/[DBNH]OAc solutions extruded at a speed of 3.5, 5.2 and 5.7 m/min with 100 and 150 µm spinneret and subjected to a draw ratio of 1.5 (Paper IV).

Table 5.2. Spinning parameters, zero-shear viscosity and calculated elongational viscosity of 13 wt-% B-PHK/[DBNH]OAc solutions.

Spinneret	Extrusion velocity	Spinning Temperature	Zero-shear viscosity*	Elongational viscosity
	m/min	°C	Pa.s	Pa.s
36 x 150 μm - L/D 0.2	5.2	76	31 955	42 000
36 x 100 μm - L/D 0.2	3.5	76	27 100	96 000
36 x 100 μm - L/D 0.2	5.7	75	27 868	82 000

*calculated from oscillatory shear measurement

The diameter of the spinneret capillary demonstrated a significant influence on the calculated elongational viscosity. An increase in diameter of 50% resulted in a drop of about 48.6% in the elongational viscosity. A wider spinneret capillary corresponds to a larger solution throughput and thus a slower cooling of the fluid filament, which undergoes a slower rise of the extensional viscosity along the air gap. The extrusion speed seems to have a lower effect on the extensional viscosity. A viscosity of 82 000 Pa.s was calculated with a velocity of 5.7 m/min while a value of 96 000 Pa.s was obtained with a speed of 3.5 m/min. At lower extrusion velocity, the filaments spend more time in the air gap which also implies more time to cool down, resulting in an increase of the elongational viscosity.

The ratio of the elongational and zero-shear viscosity (Trouton ratio) shows relatively low values, particularly the ratio from the experiment using the 150 μm spinneret. These results may come from the simplifications made by Boerstoel on the velocity of the fluid filament in the air gap and the assumptions in the resulting force balance that might not be valid (Boerstoel 1998). Boerstoel neglects the gravitational, friction, surfacial and inertial forces in the force balance considering them to be small for high viscous materials compared to the external and rheology forces. Other studies demonstrate the potential importance of these forces in the calculation of the extensional properties of a material (Szabo 1997, Szabo, McKinley 2003). Furthermore, the low draw ratio used in these experiments (DR 1.5) results in relatively thick fluid threads in the air gap and may increase the gravitational, inertial and surfacial effects. Under these conditions, the assumption of neglecting them may not be valid.

5.3 Dry-jet wet spinning of cellulose/ionic liquid solution

5.3.1 Spinnability of cellulose/[EMIM]OAc solution

Despite its efficient capability of dissolving cellulose, [EMIM]OAc showed very poor spinnability. A stable and clear extrusion of cellulose/[EMIM]OAc solution, varying from 8 to 15 wt-%, was impossible to achieve. Figures 5.11 (A and B) illustrate the phenomena observed on the surface of the spinneret and in the

air gap after extrusion. The first instability, exhibited in Figure 5.11 A), corresponds to the merging of several filaments forming viscous drops and preventing the establishment of clear extrusions and drawing of the filaments. In this case, the viscous properties seemed to dominate the elastic properties. By decreasing the spinning temperature, single filaments were obtained. However, an irregular outflow due to melt fracture (Figure 5.11 B)) originating from an inappropriate spinneret geometry was noticed and restrained the stretching of the filaments.

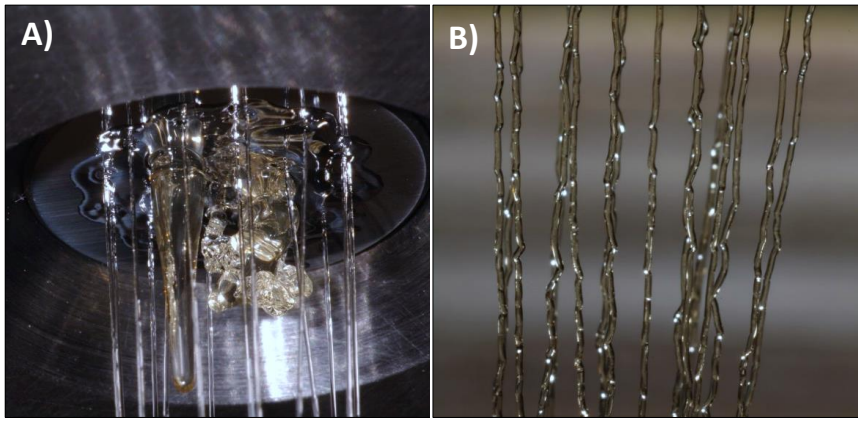

Figure 5.11. Extrusion instabilities of E-PHK/[EMIM]OAc solutions. A) Drop formation, B) irregular outflow due to melt fracture caused by inappropriate spinneret geometry.

5.3.2 Spinnability of cellulose/[DBNH]OAc solution

[DBNH]OAc exhibited very good solvent properties as well as excellent spinnability. Figure 5.12 depicts the extrusion appearance of a 13 wt-% B-PHK/[DBNH]OAc solution. By varying the extrusion temperature, the optimum viscoelastic properties for E-PHK and B-PHK pulps were identified and set to a zero-shear viscosity of about 30 000 Pa.s and a COP located at an angular frequency around 1 s^{-1} and a modulus between 4 000 - 5 000 Pa.

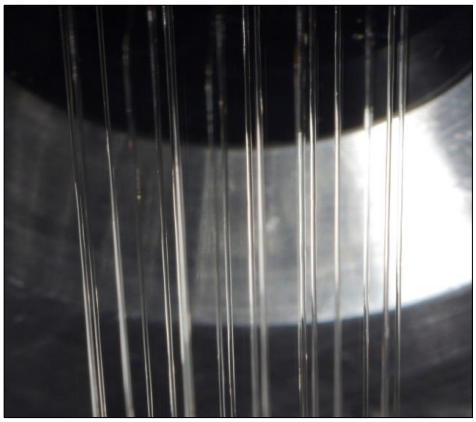

Figure 5.12. Extrusion of a 13 wt-% B-PHK/[DBNH]OAc solution.

5.3.2.1 Influence of cellulose MMD on the spinnability and fiber properties (Paper III)

The cellulose blend/[DBNH]OAc solutions presented in chapter 5.2.1.3 were spun by dry-jet wet spinning. Table 5.3 summarizes the spinning temperatures at which the different polymer solutions were extruded, as well as the maximum possible draw ratio applied to the filaments.

Table 5.3. Dry-jet wet spinning conditions of cellulose blends and reference pulp E-PHK /[DBNH]OAc solutions extruded at 5.7 m/min (Paper III).

	Concentration	**$T_{spinning}$**	**Zero-shear viscosity**	**Maximum DR**
	wt-%	°C	$Pa.s^{-1}$	-
Blend 1	15	80	31 000	3.0
Blend 2	15	75	35 729	15.0
Blend 3	15	79 - 82	36 641	-
Blend 4	13	70	25 565	1.5
	15	80 - 85	33 830 - 26772	-
Blend 5	15	75	28 827	3.0
Blend 6	13	70	28 752	15.0
	15	85 - 87	30 347	3.0
E-PHK	13	75	27 971	15.0
	15	85	38 034	15.0

Clear and stable extrusions, without the formation of filament agglomerations, were obtained for all [DBNH]OAc solutions. However, the spinnability, which is reflected by the maximum draw ratio, differed significantly from one solution to another. The starting spinning temperature for each blend was selected to reach a zero-shear viscosity similar to the one employed for the spinning of E-PHK pulp (30 000 Pa.s). In case of unsuccessful spinning, the extrusion temperature was varied to seek for more stability. Despite comparable zero-shear viscosity, only blends 2 and 6 demonstrated sufficient spinnability at an extrusion velocity of 5.7 m/min and could be stretched at high draw ratios (DR 15) without any filament breaks. Blends 1, 3, 4 and 5, despite stable extrusions, could not be drawn to a high extent: frequent filament breaks occurred at the entrance of the coagulation bath and were amplified by the increase of the draw ratio, preventing the take-up of the filaments and collection of samples. The colored dots in Figures 5.7 A) and B) denote the rheological conditions at which the different blend solutions were spun. The green dots refer to successful spinning (high draw applicable), orange dots correspond to intermediate spinning (low draw applicable) and red dots to unsuccessful spinning (no draw achievable). The different responses of the spun solutions under similar process conditions emphasize the importance of the viscoelastic properties of cellulose/[DBNH]OAc solutions and, therefore, the significance of cellulose MMD to achieve effective spinning. The viscoelastic properties of a solution (zero-shear viscosity, angular frequency and dynamic modulus of the COP) require to be within specific ranges to obtain successful spinning. According to this study, the following matrix was identified: zero-shear viscosity between 27 000 and 40 000 Pa.s, angular frequency of COP between 0.8 and 1.5 s^{-1} and dynamic modulus of COP between 3 000 and 6 000 Pa. The validity of this matrix was confirmed with the reduction of the dynamic modulus of blends 4 and 6 via the decrease of the concentration from 15 wt-% to 13 wt-%, which resulted in an improvement of the maximum draw ratio.

In terms of MMD, the spinnability of cellulose/[DBNH]OAc solutions demonstrated a close relationship with the share of high molecular weight cellulose fraction and with the polydispersity index (PDI). A proportion of cellulose chain of DP > 2000 larger than 20 wt-% combined with a share of cellulose chains showing a DP < 100 between 3 and 7 wt-% resulted in excellent spinnability with high stretching. The presence of longer chains favor uniform and homogeneous interactions between polymer chains during the solution extrusion in the air gap and the formation of a more cohesive cellulose network during the regeneration process in the coagulation bath. This developed cellulose structure directly enhances the elongational properties of the fluid filament and reduce the occurrence of filament breaks.

The properties of the fibers collected during the successful spinning are presented in Figures 5.13 and 5.14 as a function of the draw ratio. The total orientation and the mechanical properties of the fibers spun from blends 2 (15 wt-%)

and 6 (13 wt-%) exhibited comparable properties with the fibers spun from the commercial E-PHK.

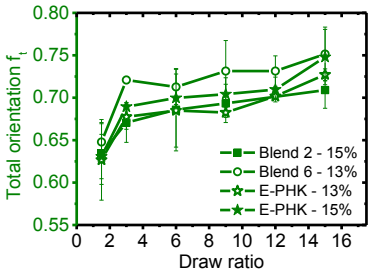

Figure 5.13. Total orientation of the fibers spun from blends 2 and 6 and E-PHK/[DBNH]OAc solutions as a function of draw ratio (Paper III).

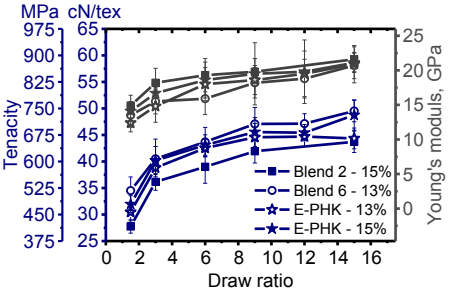

Figure 5.14. Tenacity and Young's modulus of the fibers spun from blends 2 and 6 and E-PHK/[DBNH]OAc solutions as a function of draw ratio (Paper III).

The large share of high molecular weight cellulose present in solution allows for the collection of fibers at high draw ratios. The alignment of the cellulose chains in the air gap promotes the formation of a more cohesive fiber network and results in thinner and higher tenacity fibers. The presence of long cellulose chains favors the creation of a more uniform and homogeneous structure which generates stronger fibers. As a consequence, the elongation at break is reduced as the generation of a highly oriented cellulose structure prevents the chains to slide along each other. The slightly higher tenacity of blend 6 over blend 2 may be explained by the lower PDI of the former implying a smaller share of low DP (<100) cellulose chains for a similar high molecular weight cellulose fraction (DP>2000). The mechanical properties of the fibers produced from blend 6 and E-PHK show similar values whereas the fibers from blend 2 demonstrate slightly lower values. E-PHK and blend 6 exhibit comparable cellulose MMD and PDI (Figure 5.6) with a relatively pronounced high molecular weight cellulose fraction (27.2 and 22.5 %) and an intermediate PDI (3.4 for both). Blend 2 also has an important share of long chains (23.9 %) but a broader PDI (5.9) indicating the presence of a higher amount of low molecular weight cellulose, DP < 100 (6.9 % instead of 3.5 and 3 % for E-PHK and blend 6, respectively). The higher proportion of short chains may result in a less uniform and oriented cellulose network and thus weaker fiber. The combination of a large fraction of high molecular weight cellulose and an intermediate PDI appeared to favor spinnability and the manufacture of stronger fibers.

5.3.2.2 Influence of process parameters on spinnability and fiber properties

5.3.2.2.1 Influence of the draw ratio on the filament structure formation

The orientation of the cellulose chains occured mainly in the air gap between the spinneret and the surface of the coagulation bath due to the external extensional tension exerted on the filaments. The increase of the draw ratio resulted

in a rise of the orientation of the polymer chains within the filaments, as depicted in Figure 5.15. As noticed, the orientation is developed rapidly at low draws and reaches a plateau at draw ratio of about 6. Only a small draw was thus necessary to produce highly oriented fibers, spun from a 13 wt-% B-PHK/[DBNH]OAc solution with a 100 µm spinneret. The Young's modulus and tenacity of the fibers are closely related to the orientation of the cellulose chains and showed a similar trend, as shown in Figures 5.15 and 5.16, respectively. High tenacity fibers of about 50 cN/tex and Young's modulus of about 20 GPa could be produced already at a draw of 6. On the contrary, the elongational properties of the resulted fibers decreases with an increase of the draw ratio, as the cellulose structure is more packed and the cellulose chains are not able to slide past each other anymore (Figure 5.16). The increase of the draw ratio results in the reduction of the diameter or titer of the fibers (Figure 5.17). A draw of 15 resulted in fibers of 11 µm diameter (1.4 dtex). Fibers of a large range of properties can thus be produced by varying the amount of stretching.

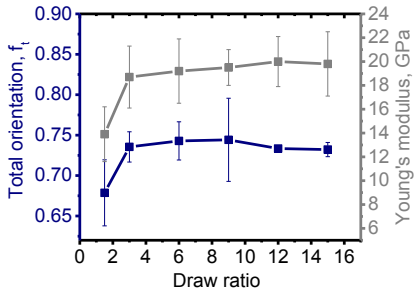

Figure 5.15. Evolution of the total orientation and Young's modulus as a function of draw ratio of fibers spun from a 13 wt-% B-PHK/[DBNH]OAc solution with a 100 µm spinneret.

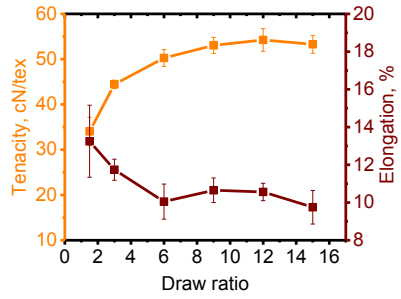

Figure 5.16. Evolution of the tenacity and elongation as a function of draw ratio of fibers spun at from a 13 wt-% B-PHK/[DBNH]OAc solution with a 100 µm spinneret.

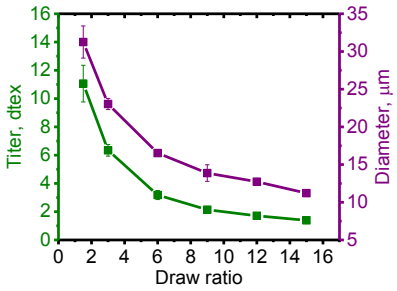

Figure 5.17. Evolution of the titer and calculated diameter as a function of draw ratio of fibers spun from a 13 wt-% B-PHK/[DBNH]OAc solution with a 100 µm spinneret.

5.3.2.2.2 Influence of air gap length (Paper IV)

The air gap length appeared to have no significant influence on the finess and mechanical properties of fibers spun from a 13 wt-% B-PHK/[DBNH]OAc solution at a draw ratio of 1.5 with a 100 µm spinneret at an extrusion velocity of 3.5 m/min. Table 5.4 summerizes the properties of the collected fibers for air gaps ranging from 1 to 3.5 cm. Only a minor decrease in the tenacity and consequently a slight increase in the elongation is noticed even though the total orientation of the chains does not show a clear decrease with the extension of the air gap length.

Table 5.4. Fineness and tensile properties of fibers spun from a 13 wt-% B-PHK/[DBNH]OAc solution at a temperature of 76 °C with a 36 holes, 100 µm, L/D 0.2 spinneret at an extrusion of 3.5 m/min and draw ratio of 1.5.

Air gap length cm	Titer, dtex	±	Total orientation	±	Tenacity cN/tex	±	Elongation %	±	Young's modulus GPa	±
1.0	12.2	0.8	0.623	0.020	33.2	1.9	14.8	1.5	14.9	1.8
1.5	12.6	0.6	0.601	0.006	32.0	1.6	17.4	1.2	13.4	1.3
2.0	12.6	0.9	0.618	0.019	29.4	2.0	16.3	1.9	14.1	1.8
2.5	12.6	1.1	0.632	0.022	28.2	2.6	16.6	1.5	13.2	1.5
3.0	12.6	1.2	0.659	0.019	28.5	2.3	18.4	1.6	13.1	1.4
3.5	12.4	1.2	0.583	0.023	28.2	2.5	18.4	2.8	13.9	2.2

5.3.2.2.3 Influence of the temperature of extrusion on spinnability

As explained in chapter 5.2.1.2, the viscoelastic behaviour of a cellulose/IL solution changes according to its temperature. Table 5.5 shows the predominance of the viscous property over the elastic one upon the rise of the process temperature during the spinning of a 13 wt-% B-PHK/[DBNH]OAc solution (unpublished data). The reduction in the zero-shear viscosity and the shift of the COP between the loss and storage moduli illustrate the drift of the solution

properties toward more pronounced viscous behavior. The impairment of the ability of the fibers to be stretched during processing originates from the more liquid-like behavior of the solution. The augmentation of filament breaks when increasing the process temperature prevented the drawing and collection of fibers. A certain elasticity of the solution is thus required to achieve stable spinning.

Table 5.5. Influence of the viscoelastic properties of a 13 wt-% B-PHK-[DBNH]OAc solution at temperatures between 80 and 90 °C on the maximum spinning draw ratio.

T_{spin}	Zero-shear viscosity	Angular frequency at COP	Dynamic modulus at COP	DR_{max}
°C	Pa.s	Pa	s^{-1}	
80	32468	0.83	4656	17.7
82	28585	0.92	4569	12.4
83	26659	1.00	4578	7.1
84	25540	1.10	4682	7.1
85	20210	1.27	4554	3.6
90	16280	1.81	4733	2.7

5.3.2.2.4 Influence of the extrusion velocity (Paper IV)

The increase of the extrusion velocity (spinning of a 13 wt-% B-PHK/[DBNH]OAc solution, 75 °C, 100 µm spinneret) from 3.5 m/min to 5.7 m/min did not demonstrate a significant influence on the orientation of the cellulose chains and resulting mechanical properties, as observed in Figures 5.18 and 5.19. Due to technical limitations in the take-up velocity, only a maximum draw of 15 could be set at an extrusion velocity of 5.7 m/min whereas a maximum draw of 25 could be reached at a speed of 3.5 m/min. Only a slight rise in the tenacity is noticed at a speed of 5.7 m/min which might be due to the augmented shear stress in the spin capillary. These results confirm the trend found by Mortimer et al. on the increase of the extrusion velocity in the spinning of NMMO-Lyocell fibers (Mortimer, Peguy et al. 1996).

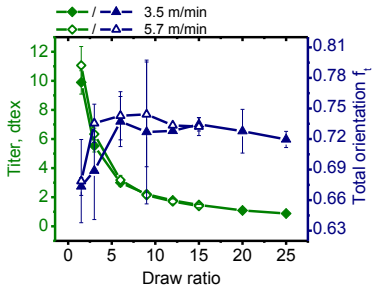

Figure 5.18. Titer and total orientation as a function of draw ratio of fibers spun at extrusion velocities of 3.5 and 5.7 m/min with a 100 µm spinneret from a 13 wt-% B-PHK/[DBNH]OAc solution (Paper IV).

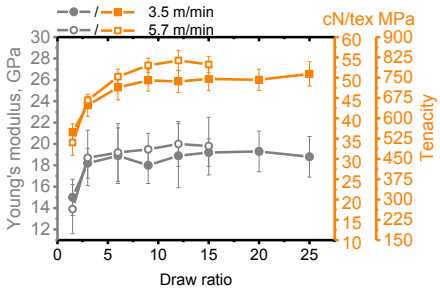

Figure 5.19. Young's modulus and tenacity as a function of draw ratio of fibers spun at extrusion velocities of 3.5 and 5.7 m/min with a 100 µm spinneret from a 13 wt-% B-PHK/[DBNH]OAc solution (Paper IV).

5.3.2.2.5 Influence of the spinneret capillary diameter (Paper IV)

The diameter of the spinneret capillary demonstrated a major effect on the diameter and associated titer of the spun fibers. The production of low titer fiber required higher draw ratios with larger spinnerets as the volumetric flow is increased. A draw of 2.5 was needed with a 100 µm spinneret to obtain a titer of about 6 dtex while with the 150 and 200 µm spinnerets, draws of about 7 and 12, respectively, were necessary (Figure 5.20). No significant influence of the spinneret nozzle diameter on the total orientation of fibers spun from a 13 wt-% B-PHK/[DBNH]OAc was observed, as exhibited in Figure 5.21. Nevertheless, slightly lower tenacities of the fibers spun with a 200 µm spinneret are noticed with a maximum of 46 cN/tex whereas tenacities of 50 cN/tex were achieved with the 100 and 150 µm spinnerets. Mortimer et al. reported larger influence of the spinneret diameter on the mechanical properties of NMMO-Lyocell fibers (Mortimer, Peguy et al. 1996).

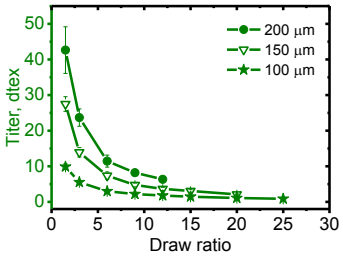

Figure 5.20. Titer as a function of draw ratio of filaments spun with 100, 150 and 200 µm spinnerets from a 13 wt-% B-PHK/[DBNH]OAc solution at an extrusion velocity of 5.7 m/min (Paper VI).

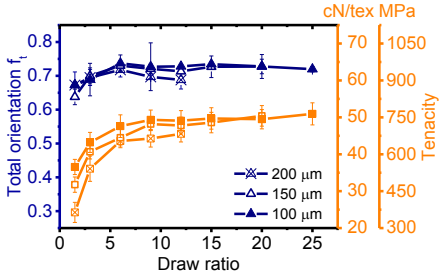

Figure 5.21. Total orientation and tenacity as a function of draw ratio of filaments spun with 100, 150 and 200 µm spinnerets from a 13 wt-% B-PHK/[DBNH]OAc solution at an extrusion velocity of 5.7 m/min (Paper IV).

5.3.2.2.6 Influence of the coagulation bath temperature on the regeneration process (Paper IV)

The temperature of the aqueous coagulation bath demonstrated a very important influence on the regeneration of cellulose filament. The influence of the bath temperature was investigated by gradually increasing the temperature from 15 to 30 °C. Fibers could be collected only at 15, 20 and 23 °C at draws ranging from 1.5 to 15. A temperature higher than 25 °C prevented the stretching and the collection of filaments. The total orientation and the tenacity of the collected fibers are depicted in Figure 5.22. The differences in fiber properties are solely related to the intrinsic response of the oriented cellulose network within the fluid filament when entering the aqueous bath, as the other process parameters were kept constant (13 wt-% B-PHK/[DBNH]OAc solution, 100 µm spinneret, extrusion velocity 5.7 m/min, air gap 1 cm). The fibers regenerated in a bath at 15 °C demonstrate slightly higher orientations and tenacities than the fibers regenerated at 20 and 23 °C. In a colder bath, the diffusion coefficient of the solvent, from the cellulose solution into the non-solvent, is lowered. No effect of the bath temperature is observed at a draw of 1.5. The moderate orientation of the cellulose chains at that draw might explain the small extent of chain relaxation in the spinning bath. The collection of fibers was impossible at temperature higher than 25 °C due to the constant break of the filaments occurring in the bath even at low draw. These failure might result from the skin-core structure of the filament formed during regeneration which breaks if the tension generated within the filament and transmitted to the solid-liquid boundary becomes too prominent. Colder bath may cause the development of a stronger liquid core which shows more resistance toward deformation. On the contrary, higher bath temperatures reduce the maximum stress tolerated by the liquid core structure and promote failure.

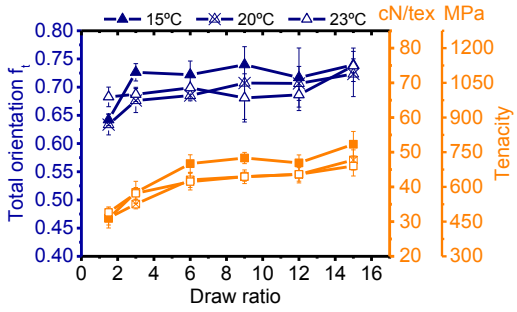

Figure 5.22. Total orientation and tenacity as a function of draw ratio of filaments coagulated in water at 15, 20 and 23 °C, spun from a 13 wt-% B-PHK/[DBNH]OAc solution extruded at a velocity of 5.7 m/min with a 100 µm spinneret (Paper IV).

5.4 Production of high tenacity fibers for textile purposes

5.4.1 Ioncell-fibers as alternative to viscose and Tencel® fibers

E-PHK and B-PHK/[DBNH]OAc solutions demonstrated excellent spinning processability and resulted in the production of high tenacity fibers. The mechanical properties of the Ioncell fibers are compared with the properties of the commercial viscose and Tencel® fibers in Table 5.6. The listed viscose fiber properties correspond to the standard viscose fibers (CV) for textile and nonwoven applications. Several fiber quality are accessible via the viscose process by varying the process conditions (Röder, Moosbauer et al. 2013) but are not included in the comparison. Ioncell fibers exhibit superior tenacities and thus lower elongations (conditioned and wet state) than the commercial fibers with tenacities over 45 cN/tex and elongation at break around 10%. The Ioncell-F process is a Lyocell-type process in which the polymer solution is spun through an air gap and regenerated in water. The resulting fiber properties follow hence the same trend as the Tencel® fibers. High tenacities are achieved and preserved in wet state due to the high orientation of the fibers. The elongation at break of the Ioncell fibers can be enlarged by applying lower draw ratios during spinning, which would reduce the resulting orientation of the cellulose chains and tenacity.

Table 5.6. Properties of the commercial viscose and Tencel® fibers (Röder, Moosbauer et al. 2009), and Ioncell-fibers.

	Viscose (CV)	Tencel®	Ioncell-F*
Titer, dtex	1.4	1.3	1.5
Tenacity cond., cN/tex**	23.9 (ca 360 MPa)	40.2 (ca 600 MPa)	45.6 (ca 684 MPa)
Elongation cond., %	20.1	13.0	8.9
Tenacity wet, cN/tex	12.5 (ca 187 MPa)	37.5 (ca 560 MPa)	42.4 (ca 636 MPa)
Elongation wet, %	22.0	18.4	11.3

*from 13 wt-% B-PHK/[DBNH]OAc solution. **conditionned: 23 °C and 50% relative humidity.

The cross-sectional structure of the spun Ioncell fibers has been characterized by scanning electron microscopy (SEM) and is illustrated in Figure 5.23. As produced via a Lyocell-type process, the observed morphology is similar to Tencel® fibers that is represented by a smooth fiber surface, round cross section, and homogeneous and dense fibrillar structure (Röder, Moosbauer et al. 2013). Furthermore, it is expected that the Ioncell fibers would behave similarly toward mechanical abrasion as Tencel® fibers and tend to fibrillate due to the high orientation of the cellulose chains (Paper II).

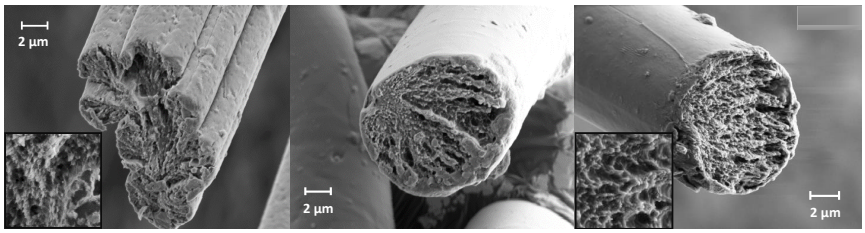

Figure 5.23. SEM images of viscose (left), Tencel® (middle) and Ioncell-fiber (right). The insets in the left corners show a 2.8 and 2.5 times magnification of the body of the viscose and Ioncell fiber, respectively (Paper II).

5.4.2 Production of Ioncell-F fabrics and garments

The suitability of the Ioncell-F process, employing [DBNH]OAc as cellulose solvent, for the production of man-made cellulosic fibers for textile purposes was investigated via the manufacture of knitted and woven fabrics. For that purpose, three demonstration runs were conducted. The staple fibers and final products were produced at Aalto University, Finland, while the yarns were manufactured at the University of Borås, Sweden (Paper II).

5.4.2.1 Production of staple fibers

The Ioncell fibers produced for the three demonstration runs (DeR1, DeR2 and DeR3) were all spun from 13 wt-% cellulose/[DBNH]OAc solutions. E-PHK pulp was employed as starting materials in DeR1 whereas B-PHK pulp was used in DeR2 and DeR3. The properties of the spun staple fibers are summarized in Table 5.7. The strength superiority of the Ioncell fibers over the commercial viscose fibers is demonstrated in Figure 5.24, representing the measured stress-strain curves of the Ioncell and viscose fibers.

Table 5.7. Properties of the produced Ioncell fibers.

	DeR1	DeR2	DeR3
Linear density (dtex)	1.9 ± 0.3	1.7 ± 0.2	1.5 ± 0.2
Cond.* tenacity (cN/tex)	46.3 ± 3.2	48.3 ± 4.6	45.6 ± 4.7
Cond. elongation (%)	9.4 ± 1.1	8.8 ± 1.0	8.9 ± 1.7
Cond. Young's modulus (GPa)	23.4 ± 3.5	20.9 ± 3.1	20.6 ± 3.7
Wet tenacity (cN/tex)	42.6 ± 3.6	44.1 ± 4.6	42.4 ± 3.6
Wet elongation (%)	11.7 ± 1.3	11.6 ± 1.2	11.3 ± 0.7
Total orientation	0.676 ± 0.042	0.730 ± 0.035	0.677 ± 0.078

*Conditionned: 23 °C and 50% relative humidity.

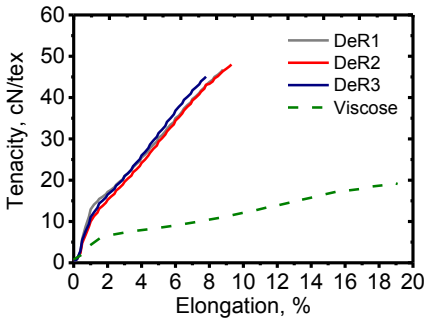

Figure 5.24. Stress-strain curves of viscose and Ioncell fibers.

The bundle of filaments of 30 cm length collected from the take-up godet, were cut into staple fibers of 4 cm length, washed offline at 70 °C in hot water for 1h and air dried without tension to induce a small natural crimp to the fibers. No spin finish was used on the wet fibers. Preliminary test to assess the amount of residual IL in the produced fibers were conducted via elemental analysis. A content of less than 1% was determined. However, more representative values will be available once the final spinning (and after-treatment) protocol has been established.

5.4.2.2 Conversion of the Ioncell fibers into yarns

Staple fibers were converted into doubled (two-ply) yarns by means of a lab mini spinning line comprising carding, drafting/roving, ring spinning and plying/winding units, as illustrated in Figure 5.25. For comparison purpose, viscose two-ply yarn were also manufactured from commercial staple viscose fibers (CV).

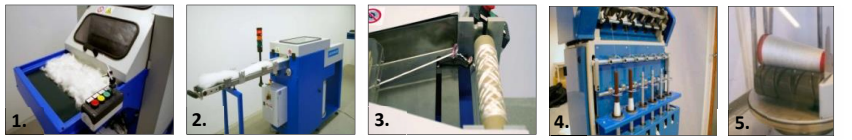

Figure 5.25. Process steps of the manufacture of two-ply yarn: 1. laboratory carding machine, 2./3. stiro Roving lab, 4. Ring lab Fibers, 5. AGTEKS DirectTwist 2A.

The properties of the resulting yarn are listed in Table 5.8. The linear density of the two-ply yarn was doubled in DeR3 as the produced yarn was intended for weaving during which the tension applied to the yarn is greater. The relatively high coefficient of variation CV and irregularity index I are explained by the variation of the fiber fineness arising from the processing fluctuation in laboratory scale and by the fiber length variation due to the manual cutting of the filament to staple fibers. The Ioncell yarns show tenacities approximately as twice higher as the viscose yarn and consequently elongations reduced by half.

Table 5.8. Properties of viscose and Ioncell two-ply yarns.

	Viscose	DeR1	DeR2	DeR3
Yarn count (tex)	31.5 tex × 2	27 tex × 2	25.5 tex × 2	49 tex × 2
Tenacity (cN/tex)	17.3 ± 1.6	34.4 ± 3.8	33.2 ± 5.1	28.5 ± 2.8
Elongation (%)	18.2 ± 1.1	7.4 ± 0.7	7.5 ± 0.7	7.9 ± 0.4
CV (%)	9.1	13.6	15.4	9.8
Fibre count/yarn cross section	418	286	299	661
Irregularity index I	1.86	2.29	2.66	2.51

5.4.2.3 Production of knitted and woven garments

The resulting yarns were dyed with Remazol reactive dyes which are widely employed on industrial scale. Bright colors from light yellow to black could be successfully obtained, attesting the good dyeability of the Ioncell fibers. The dyed yarn from DeR1 and DeR2 were knitted into a scarf and a dress, as depicted in Figure 5.26 a) and b) with a stoll CMS 340 TC-L multi-gauge flatbed knitting machine. The scarf was designed by Marjanna Tanttu from Aalto University and the dress by Tuula Pöyhönen from the Finnish design company Marimekko. The knitted garment from DeR2 (dress) demonstrated higher evenness in the structure of the fabric and softer touch due to the greater homogeneity and fineness of the starting staple fibers. The Ioncell yarn from DeR3 was woven into a bowtie and pocket handkerchief by Eveliina Netti from Aalto University (Figure 5.26 c)). The rare breaks observed during weaving attested the strength of the produced yarn. Both the Ioncell knitted and woven fabrics showed low hairiness and a shiny aspect without any additional spinning finish after-treatment.

Figure 5.26. Garments manufactured during the three demonstration runs. a) DeR1: knitted scarf, b) DeR2: knitted dress, c) DeR3: Woven bowtie and pocket handkerchief (Paper II).

The yarn evenness was also estimated and compared visually by knitting a sample (Figure 5.27) of undyed Ioncell (DeR1 and DeR2) and viscose two-ply yarns. The unevenness of a fabric can be described by the presence of horizontal stripes on the knitted garment. These stripes originate from the inhomogeneity of the spun yarn due to the uneven fineness of the staple fibers along the yarn and the variation of the number of fibers in the yarn cross-section. The lower linear density, higher strength and more homogeneous fiber density and length achieved in DeR2 resulted in the better evenness of the knitted spun yarn in comparison with DeR1. As observed in Figure 5.27, the appearance of the DeR2 sample is similar to the viscose knitted sample apart from the whiter aspect of the latter due to the after-treatment applied to the fibers during the production process. The few stripes observed on the knitted viscose and DeR2 samples suggest that some of the irregularities in the two-ply yarn could be a result of the yarn production process which has not been thoroughly optimized yet.

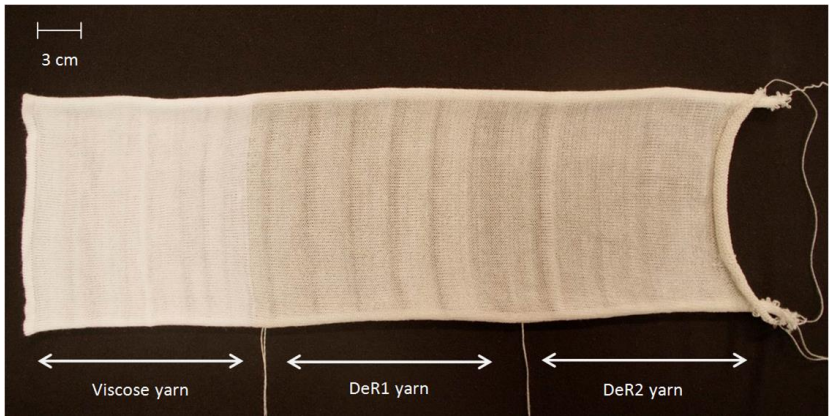

Figure 5.27. Knitted sample from viscose and Ioncell (DeR1 and DeR2) two-ply yarn (Paper II).

6. Concluding remarks

A new technology for the production of man-made cellulosic fibers by dry-jet wet spinning, employing a novel ionic liquid as cellulose solvent, was investigated in the present study. This Ioncell-F process was developed as a potential new alternative to fill the future cellulose gap, which is expanding due to the growing world population and level of prosperity.

The two ionic liquids tested during this work, 1-ethyl-3-methylimidazolium acetate and 1,5-diazabicyclo[4.3.0]non-5-enium acetate, demonstrated contrasting spinning behavior, the former showing poor spinning capability, despite similar efficiency in dissolving cellulose. It was observed that mild temperature, low shearing rate and low vacuum minimized the depolymerization of cellulose during its dissolution in both ILs. Capillary breakup extensional rheology and oscillatory shear rheology appeared to be suitable methods to monitor the extent of the degradation of cellulose dissolved in ILs, due to the relationship between the viscoelastic properties of the IL solution and the MMD of the dissolved cellulose. A reduction in cellulose DP enhances the viscous behavior of the solution, which can be followed by the breakup time of the fluid subjected to extensional tension, or the variation of the solution dynamic viscosity and moduli when subjected to shear stress.

The spinnability of cellulose/[DBNH]OAc solutions displayed tight connection to its viscoelastic behavior. A specific matrix of viscoelastic properties to achieve optimal spinnability was identified. The value of the zero-shear viscosity and the modulus and angular frequency of the cross-over point between the loss and storage moduli need to be in particular ranges. The presence of a certain share of high molecular weight cellulose (DP>2000) and intermediate cellulose polydispersity led to adequate rheological conditions for favorable processing. Within these conditions, the ability of the polymer solution to be stretched in the air gap without any kind of break was significantly improved. Long cellulose chains contributed to the stability of the fluid filament in the air gap, and to the formation of a more cohesive cellulose network that could resist the external elongational tension and prevent filament breaks.

A novel method was presented to determine the elongational viscosity of the highly viscous cellulose solution via the online measurement of the force acting on the filament tow at the exit of the coagulation bath. The assessment of the elongational viscosity of a fluid is primordial in air gap spinning, as the liquid

thread is subjected to substantial extensional tension in the air gap. Valuable results were obtained, but further thorough investigation is required to establish an accurate relationship between the elongational viscosity of the IL solution and the process parameters.

The spinning window required to achieve continuous spinning was established by investigating the influence of the main process parameters on the spinnablity and mechanical properties of the resulting fibers. The variation of the draw ratio and temperature of the coagulation bath showed a significant effect on the creation of a strong cellulose structure within the filament and hence, on the mechanical properties. The extrusion velocity, air gap length and nozzle diameter demonstrated only a minor influence on the structural and mechanical properties. Fibers exhibiting low diameter and high mechanical properties were produced via high drawing of the liquid thread in the air gap and its coagulation in a cold aqueous bath. Fibers having higher elongation at break could be also manufactured by applying lower draw ratios, which created a less-packed network and permitted the cellulose chains to extend more freely.

Ioncell fibers were proven to be competitive textile fibers against the viscose and Lyocell fibers. Ioncell two-ply yarn was successfully produced from Ioncell staple fibers, then dyed and knitted or woven to fabrics. The production of garments attests to the fitness of the Ioncell fibers for textile applications. The resulting fabrics presented evenness, a shiny look and light feeling that was comparable to viscose or Tencel® garments.

To conclude, this work presented the first steps in the development of a new spinning process for the production of cellulosic fibers from ionic liquid. The essential spinning concepts (primordial for the establishment of a new technology) were investigated and led to the identification of the spinning window required to achieve stable spinning and produce high quality fibers for textile purposes. The fundamental relationships between the intrinsic characteristics of the starting material, the rheological behavior of the spinning solution, spinnability and properties of the resulting fibers were established (Figure 6.1). This work constitutes a base for the Ioncell-F process and will greatly contribute to its further development and up-scaling.

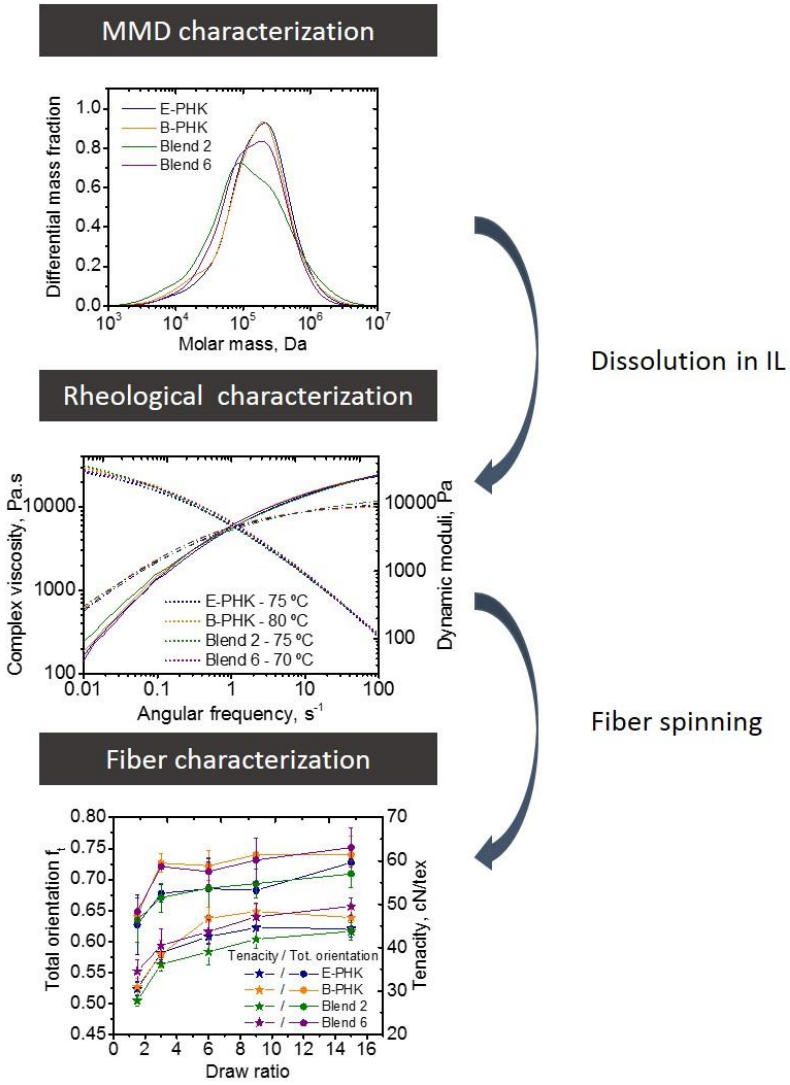

Figure 6.1. Fundamental steps of the Ioncell-F process and their interconnection.

7. Future work and outlook

This work is part of a very challenging project with the goal to develop a sustainable bioeconomy in Finland relying on the use of renewable resources to produce food, energy, and high-value products and services. The rise in environmental awareness drives the transition of the present industry towards new technologies, presenting a less harmful impact on the environment by employing biomass as raw materials, cleaner technologies and efficient recycling of materials.

The development of the Ioncell-F process has been carried out according to the bioeconomy strategy. To fulfil the requirements, a detailed economic study of the full concept has to be conducted to determine the implementation requirements of the process on an industrial scale. The principal questions and challenges to fully realizing this sustainable bioeconomy strategy are:

- Recovery of the ionic liquid from the coagulation bath to establish a closed-loop process
- Achievement of a recovery rate of more than 99%, to make the process industrially viable
- Reduction of the energy required to separate the IL from the water
- Production of high-purity IL after the recycling steps
- Capability of the recycled IL to dissolve cellulose after several recycling steps
- Optimal spinnability of polymer solutions prepared from recycled IL
- Production of high-quality fibers from recycled IL and recycled cellulose waste

To respond to these open questions, the capacity of the spinning unit has been scaled-up and a semi-pilot scale thin film evaporator has been purchased. These aspects of the process are the focus of attention and under current investigation.

References

Adusumalli, R., Keckes, J., Martinschitz, K.J., Boesecke, P., Weber, H., Roeder, T., Sixta, H. and Gindl, W., (2009). Comparison of molecular orientation and mechanical properties of lyocell fibre tow and staple fibres. *Cellulose,* **16**(5), pp. 765-772.

Anna, S.L. and McKinley, G.H., (2001). Elasto-capillary thinning and breakup of model elastic liquids. *Journal of Rheology,* **45**(1), pp. 115-138.

Atalla, R.H. and Vanderhart, D.L., (1984). Native cellulose: a composite of two distinct crystalline forms. *Science,* **223**(4633), pp. 283-285.

Baird, D.G., (1999). The role of extensional rheology in polymer processing. *Korea-Australia Rheology Journal,* **11**(4), pp. 305-311.

Biganska, O. and Navard, P., (2005). Kinetics of precipitation of cellulose from cellulose-NMMO-water solutions. *Biomacromolecules,* **6**(4), pp. 1948-1953.

BISFA, (2009). *Terminology of man-made fibers*. Brussels: BISFA.

BISFA, (2004). *Testing methods viscose, modal, lyocell and acetate staple fibres and tows*. Brussels: BISFA.

Boerstoel, H., Maatman, H., Westerink, J. and Koenders, B., (2001). Liquid crystalline solutions of cellulose in phosphoric acid. *Polymer,* **42**(17), pp. 7371-7379.

Boerstoel, H., (1998). *Liquid crystalline solutions of cellulose in phosphoric acid for preparing cellulose yarns*, Rijksuniversiteit Groninnen.

Brandt, A., Gräsvik, J., Hallett, J.P. and Welton, T., (2013). Deconstruction of lignocellulosic biomass with ionic liquids. *Green Chemistry,* **15**(3), pp. 550-583.

Bywater, N., (2011). The Global Viscose Fibre Industry in the 21st Century - The First 10 Years. *Lenzinger Berichte,* **89**, pp. 22 - 29.

Cai, T., Zhang, H., Guo, Q., Shao, H. and Hu, X., (2010). Structure and properties of cellulose fibers from ionic liquids. *Journal of Applied Polymer Science,* **115**(2), pp. 1047-1053.

Cao, Y., Wu, J., Zhang, J., Li, H., Zhang, Y. and He, J., (2009). Room temperature ionic liquids (RTILs): A new and versatile platform for cellulose processing and derivatization. *Chemical Engineering Journal,* **147**(1), pp. 13-21.

Chen, X., Zhang, Y., Cheng, L. and Wang, H., (2009). Rheology of concentrated cellulose solutions in 1-butyl-3-methylimidazolium chloride. *Journal of Polymers and the Environment,* **17**(4), pp. 273-279.

Cho, H.M., Gross, A.S. and Chu, J., (2011). Dissecting force interactions in cellulose deconstruction reveals the required solvent versatility for overcoming biomass recalcitrance. *Journal of the American Chemical Society,* **133**(35), pp. 14033-14041.

Clasen, C., (2010). Capillary breakup extensional rheometry of semi-dilute polymer solutions. *Korea-Aust Rheol J,* **22**(4), pp. 331-338.

Clasen, C. and Petri, H., (2005). Elongational Behaviour of Dilute Polymer Solutions and the Influence of Molecular Weight and Concentration, *Proceedings of the X. International Macromolecular Colloquium* 2005, pp. 1-2.

Clasen, C., Verani, M., Plog, J.P., McKinley, G.H. and Kulicke, W., (2004). Effects of polymer concentration and molecular weight on the dynamics of visco-elasto-capillary breakup, *XIVth International Congress on Rheology* 2004, pp. 1-3.

Collier, J.R., Romanoschi, O. and Petrovan, S., (1998). Elongational rheology of polymer melts and solutions. *Journal of Applied Polymer Science,* **69**(12), pp. 2357-2367.

Collier, J., Watson, J., Collier, B. and Petrovan, S., (2009). Rheology of 1-butyl-3-methylimidazolium chloride cellulose solutions. II. Solution character and preparation. *Journal of Applied Polymer Science,* **111**(2), pp. 1019-1027.

Coulsey, H.A. and Smith, S.B., (1995). The formation and structure of a new cellulosic fiber. *Lenzinger Berichte,* **75**, pp. 51-61.

Crowhurst, L., Mawdsley, P.R., Perez-Arlandis, J.M., Salter, P.A. and Welton, T., (2003). Solvent–solute interactions in ionic liquids. *Physical Chemistry Chemical Physics,* **5**(13), pp. 2790-2794.

Doherty, T.V., Mora-Pale, M., Foley, S.E., Linhardt, R.J. and Dordick, J.S., (2010). Ionic liquid solvent properties as predictors of lignocellulose pretreatment efficacy. *Green Chemistry,* **12**(11), pp. 1967-1975.

Eckelt, J., Eich, T., Röder, T., Rüf, H., Sixta, H. and Wolf, B.A., (2009). Phase diagram of the ternary system NMMO/water/cellulose. *Cellulose,* **16**(3), pp. 373-379.

Eichinger, D., (2011). A vision to the world of cellulosic fibers in 2020. *Chemical Fibers International,* **61**(4), pp. 177.

Eichinger, D. and Eibl, M., (1995). Lenzing Lyocell - an interesting cellulose fiber for the textile industry. *Lenzinger Berichte,* **75**, pp. 41-5.

El Seoud, O.A., Koschella, A., Fidale, L.C., Dorn, S. and Heinze, T., (2007). Applications of ionic liquids in carbohydrate chemistry: a window of opportunities. *Biomacromolecules,* **8**(9), pp. 2629-2647.

Feng, L. and Chen, Z., (2008). Research progress on dissolution and functional modification of cellulose in ionic liquids. *Journal of Molecular Liquids,* **142**(1), pp. 1-5.

Fink, H., Weigel, P., Purz, H. and Ganster, J., (2001). Structure formation of regenerated cellulose materials from NMMO-solutions. *Progress in Polymer Science,* **26**(9), pp. 1473-1524.

Fourné, F., (1999). *Synthetic Fibers. Machines and Equipment, Manufacture, Properties*. Munich: Hanser.

Gardner, K. and Blackwell, J., (1974). The structure of native cellulose. *Biopolymers,* **13**(10), pp. 1975-2001.

Gavillon, R. and Budtova, T., (2007). Kinetics of cellulose regeneration from cellulose-NaOH-water gels and comparison with cellulose-N-methylmorpholine-N-oxide-water solutions. *Biomacromolecules,* **8**(2), pp. 424-432.

Gebhard, S., (2004). *A practical approach to rheology and rheometry*. 2nd edn. Federal Republic of Germany: Thermo Electron Karlsruhe GmbH.

Gindl, W., Reifferscheid, M., Adusumalli, R., Weber, H., Röder, T., Sixta, H. and Schöberl, T., (2008). Anisotropy of the modulus of elasticity in regenerated cellulose fibres related to molecular orientation. *Polymer,* **49**(3), pp. 792-799.

Glasser, W.G., Atalla, R.H., Blackwell, J., Brown JR, R.M., Burchard, W., French, A.D., Klemm, D.O. and Nishiyama, Y., (2012). About the structure of cellulose: debating the Lindman hypothesis. *Cellulose,* **19**(3), pp. 589-598.

Golzar, M., (2004). *Melt spinning of the fine PEEK filaments*. Technischen Universität Dresden.

Gordon Cook, J., (1984). *Handbook of textile fibres: man-made fibres*. 2nd edn.UK: Woodhead Publishing Limited.

Graenacher, C., (1934). *Cellulose solution*. US Patent 1943176A.

Gross, A.S. and Chu, J., (2010). On the molecular origins of biomass recalcitrance: the interaction network and solvation structures of cellulose microfibrils. *The Journal of Physical Chemistry B,* **114**(42), pp. 13333-13341.

Haemmerle, F.M., (2011). The cellulose gap (the future of cellulose fibres). *Lenzinger Berichte,* **89**, pp. 12-21.

Harms, H., (2013). Research in the Fields of Man-Made Cellulosic Fibres and Cellulose in Austria. *Lenzinger Berichte,* **91**, pp. 01-06.

Hauru, L.K., Hummel, M., King, A.W., Kilpeläinen, I. and Sixta, H., (2012). Role of solvent parameters in the regeneration of cellulose from ionic liquid solutions. *Biomacromolecules,* **13**(9), pp. 2896-2905.

Hauru, L.K., Hummel, M., Nieminen, K., Michud, A. and Sixta, H., (2015). Cellulose regeneration and spinnability from ionic liquids. *Soft Matter,* **12**, pp. 1487-1495.

Haward, S.J., Sharma, V., Butts, C.P., McKinley, G.H. and Rahatekar, S.S., (2012). Shear and Extensional Rheology of Cellulose/Ionic Liquid Solutions. *Biomacromolecules,* **13**(5), pp. 1688-1699.

Heinze, T., Dorn, S., Schöbitz, M., Liebert, T., Kölher, S. and Meister, F., (2008). Interactions of ionic liquids with polysaccharides–2: Cellulose. *Macromolecular Symposia,* **262**(1), pp. 8-22.

Hermanutz, F., Gähr, F., Uerdingen, E., Meister, F. and Kosan, B., (2008). New developments in dissolving and processing of cellulose in ionic liquids. *Macromolecular Symposia,* **262**(1), pp. 23-27.

Hong, J.H., Ku, M.K., Ahn, Y., Kim, H.J. and Kim, H., (2013). Air-gap spinning of cellulose/ionic liquid solution and its characterization. *Fibers and Polymers,* **14**(12), pp. 2015-2019.

Jiang, G., Yuan, Y., Wang, B., Yin, X., Mukuze, K.S., Huang, W., Zhang, Y. and Wang, H., (2012). Analysis of regenerated cellulose fibers with ionic liquids as a solvent as spinning speed is increased. *Cellulose,* **19**(4), pp. 1075-1083.

Kadla, J.F. and Gilbert, R.D., (20009. Cellulose structure: A review. *Cellulose Chemistry and Technology,* **34**(3-4), pp. 197-216.

Kim, D.B., Pak, J.J., Jo, S.M. and Lee, W.S., (2005). Dry jet-wet spinning of cellulose/N-methylmorpholine N-oxide hydrate solutions and physical properties of lyocell fibers. *Textile Research Journal,* **75**(4), pp. 331-341.

Kosan, B., Michel, C. and Meister, F., (2008). Dissolution and forming of cellulose with ionic liquids. *Cellulose,* **15**(1), pp. 59-66.

Langan, P., Nishiyama, Y. and Chanzy, H., (1999). A revised structure and hydrogen-bonding system in cellulose II from a neutron fiber diffraction analysis. *Journal of the American Chemical Society,* **121**(43), pp. 9940-9946.

Liebert, T., (2010). Cellulose solvents-remarkable history, bright future. *Cellulose Solvents: For Analysis, Shaping and Chemical Modification*, **1033**, pp. 3-54. American Chemical Society.

Lindman, B., Karlström, G. and Stigsson, L., (2010). On the mechanism of dissolution of cellulose. *Journal of molecular liquids,* **156**(1), pp. 76-81.

Lu, F., Cheng, B., Song, J. and Liang, Y., (2012). Rheological characterization of concentrated cellulose solutions in 1-allyl-3-methylimidazolium chloride. *Journal of Applied Polymer Science,* **124**(4), pp. 3419-3425.

Mäki-Arvela, P., Anugwom, I., Virtanen, P., Sjöholm, R. and Mikkola, J.P., (2010). Dissolution of lignocellulosic materials and its constituents using ionic liquids—A review. *Industrial Crops and Products,* **32**(3), pp. 175-201.

McKinley, G.H. and Tripathi, A., (2000). How to extract the Newtonian viscosity from capillary breakup measurements in a filament rheometer. *Journal of Rheology,* **44**(3), pp. 653-670.

Medronho, B., Romano, A., Miguel, M.G., Stigsson, L. and Lindman, B., (2012). Rationalizing cellulose (in) solubility: reviewing basic physicochemical aspects and role of hydrophobic interactions. *Cellulose,* **19**(3), pp. 581-587.

Mortimer, S. and Peguy, A., (1996a). The formation of structure in the spinning and coagulation of lyocell fibres. *Cellulose chemistry and technology,* **30**(1-2), pp. 117-132.

Mortimer, S. and Peguy, A., (1996b). The influence of air-gap conditions on the structure formation of lyocell fibers. *Journal of Applied Polymer Science,* **60**(10), pp. 1747-1756.

Mortimer, S. and Peguy, A., (1994). A device for on-line measurement of fiber birefringence. *Textile Research Journal,* **64**(9), pp. 544-551.

Mortimer, S., Peguy, A. and Ball, R., (1996). Influence of the physical process parameters on the structure formation of lyocell fibres. *Cellulose chemistry and technology,* **30**(3-4), pp. 251-266.

Mülleder, E., Schrempf, C., Rüf, H. and Feilmair, W., (1998). *Method for producing cellulose fibres*. Austria Patent WO 98/58103.

Nishiyama, Y., Langan, P. and Chanzy, H., (2002). Crystal structure and hydrogen-bonding system in cellulose Iβ from synchrotron X-ray and neutron fiber diffraction. *Journal of the American Chemical Society,* **124**(31), pp. 9074-9082.

North, M., (2013). Kelheim Fibres GmbH - A Specialist Specialises. *Lenzinger Berichte,* **91**, pp. 13-18.

Olsson, C. and Westman, G., (2013a). Direct dissolution of cellulose: background, means and applications. *Cellulose–fundamental aspects, InTech, Chapt,* **6**, pp. 144-178.

Olsson, C. and Westman, G., (2013b). Wet spinning of cellulose from ionic liquid solutions–viscometry and mechanical performance. *Journal of Applied Polymer Science,* **127**(6), pp. 4542-4548.

O'Sullivan, A.C., (1997). Cellulose: the structure slowly unravels. *Cellulose,* **4**(3), pp. 173-207.

Parviainen, A., Wahlström, R., Liimatainen, U., Liitiä, T., Rovio, S., Helminen, J.K., Hyväkkö, U., King, A.W., Suurnäkki, A. and Kilpeläinen, I., (2015). Sustainability of cellulose dissolution and regeneration in 1, 5-diazabicyclo [4.3. 0] non-5-enium acetate: a batch simulation of the IONCELL-F process. *RSC Advances,* **5**(85), pp. 69728-69737.

Paul, D., (1968). A study of spinnability in the wet-spinning of acrylic fibers. *Journal of Applied Polymer Science,* **12**(10), pp. 2273-2298.

Petrovan, S., Collier, J. and Negulesco, I., (2001). Rheology of cellulosic N-methylmorpholine oxide monohydrate solutions of different degrees of polymerization. *Journal of Applied Polymer Science,* **79**(3), pp. 396-405.

Pinkert, A., Marsh, K.N., Pang, S. and Staiger, M.P., (2009). Ionic liquids and their interaction with cellulose. *Chemical reviews,* **109**(12), pp. 6712-6728.

Plog, J.P., (2005). *Inverstigation of the visco-elastic behavior of water soluble cellulosic derivatives in uniaxial elongation.* Universität Hamburg.

Rodd, L.E., Scott, T.P., Cooper-White, J.J. and McKinley, G.H., (2005). Capillary break-up rheometry of low-viscosity elastic fluids. *Applied Rheology,* **15**, pp. 12-27.

Röder, T., Moosbauer, J., Kliba, G., Schlader, S., Zuckerstätter, G. and Sixta, H., (2009). Comparative characterisation of man-made regenerated cellulose fibres. *Lenzinger Berichte,* **87**, pp. 98-105.

Röder, T., Moosbauer, J., Wöss, K., Schlader, S. and Kraft, G., (2013). Man-made cellulose fibres - a comparison based on morphology and mechanical properties. *Lenzinger Berichte,* **91**, pp. 07 - 12.

Rogers, R.D. and Seddon, K.R., (2003). Chemistry. Ionic liquids--solvents of the future? *Science,* **302**(5646), pp. 792-793.

Rosenau, T., Potthast, A., Sixta, H. and Kosma, P., (2001). The chemistry of side reactions and byproduct formation in the system NMMO/cellulose (Lyocell process). *Progress in Polymer Science,* **26**(9), pp. 1763-1837.

Rudaz, C. and Budtova, T., (2013). Rheological and hydrodynamic properties of cellulose acetate/ionic liquid solutions. *Carbohydrate Polymers,* **92**(2), pp. 1966-1971.

Sammons, R.J., Collier, J.R., Rials, T.G. and Petrovan, S., (2008a). Rheology of 1-butyl-3-methylimidazolium chloride cellulose solutions. III. Elongational rheology. *Journal of Applied Polymer Science,* **110**(5), pp. 3203-3208.

Sammons, R., Collier, J., Rials, T. and Petrovan, S., (2008b). Rheology of 1-butyl-3-methylimidazolium chloride cellulose solutions. I. Shear rheology. *Journal of Applied Polymer Science,* **110**(2), pp. 1175-1181.

Schrems, M., Ebner, G., Liebner, F., Becker, E., Potthast, A. and Rosenau, T., 2010. Side reactions in the system cellulose/1-alkyl-3-methyl-imidazolium ionic liquid. *Cellulose Solvents: For Analysis, Shaping and Chemical Modification,* **1033**, pp. 149-164. American Chemical Society.

Singh, S. and Simmons, B.A., (2013). Ionic liquid pretreatment: mechanism, performance, and challenges. *Aqueous pretreatment of plant biomass for biological and chemical conversion to fuels and chemicals*. John Wiley & Sons, pp. 223-238.

Sixta, H., Michud, A., Hauru, L., Asaadi, S., Ma, Y., King, A.W., Kilpelainen, I. and Hummel, M., (2015). Ioncell-F: A High-strength regenerated cellulose fibre. *Nordic Pulp & Paper Research Journal,* **30**(1), pp. 43-57.

Song, J., Cheng, B., Jie, X., Liang, Y., Lu, F. and Zhang, F., (2011). Study on the coagulation process of cellulose nascent fibers with ionic liquid AMIMCl as a solvent during dry-wet spinning. *e-Polymers,* **11**(1), pp. 401-411.

Stelter, M., Brenn, G., Yarinn, A., Singh, R. and Durst, F., (2002). Investigation of the elongational behavior of polymer solutions by means of an elongational rheometer. *Journal of Rheology,* **46**(2), pp. 507-527.

Sun, N., Rahman, M., Qin, Y., Maxim, M.L., Rodríguez, H. and Rogers, R.D., (2009). Complete dissolution and partial delignification of wood in the ionic liquid 1-ethyl-3-methylimidazolium acetate. *Green Chemistry,* **11**(5), pp. 646-655.

Swatloski, R.P., Spear, S.K., Holbrey, J.D. and Rogers, R.D., (2002). Dissolution of cellose with ionic liquids. *Journal of the American Chemical Society,* **124**(18), pp. 4974-4975.

Swatloski, R.P., Rogers, R.D. and Holbrey, J.D., (2003). *Dissolution and processing of cellulose using ionic liquids*. US Patent 2003/0157351 A1 edn. USA.

Szabo, P., (19979. Transient filament stretching rheometer. *Rheologica Acta,* **36**(3), pp. 277-284.

Szabo, P. and McKinley, G.H., (2003). Filament stretching rheometer: inertia compensation revisited. *Rheologica acta,* **42**(3), pp. 269-272.

The Fiber Year Consulting, (2015). *The Fiber Year 2015: World Survey on Textile & Nonwovens*. The Fiber Year GmbH.

Wang, H., Gurau, G. and Rogers, R.D., (2012). Ionic liquid processing of cellulose. *Chemical Society Reviews,* **41**(4), pp. 1519-1537.

Wirth, B., (2011). Filament breaches during air-gap spinning. *Chemical Fibers International,* **61**(1), pp. 38.

Woodings, C., (2001). *Regenerated Cellulose Fibres*. UK: Woodhead Publishing limited.

Zhang, L., Ruan, D. and Gao, S., (2002). Dissolution and regeneration of cellulose in NaOH/thiourea aqueous solution. *Journal of Polymer Science Part B: Polymer Physics,* **40**(14), pp. 1521-1529.

Zhu, S., Wu, Y., Chen, Q., Yu, Z., Wang, C., Jin, S., Ding, Y. and Wu, G., (2006). Dissolution of cellulose with ionic liquids and its application: a mini-review. *Green Chem.,* **8**(4), pp. 325-327.

Ziabicki, A., (1976). *Fundamentals of fibre formation*. John Wiley & Sons.

Aalto-DD 90/2016

ISBN 978-952-60-6804-6 (printed)
ISBN 978-952-60-6805-3 (pdf)
ISSN-L 1799-4934
ISSN 1799-4934 (printed)
ISSN 1799-4942 (pdf)

Aalto University
School of Chemical Technology
Department of Forest Products Technology
www.aalto.fi

BUSINESS + ECONOMY

ART + DESIGN + ARCHITECTURE

SCIENCE + TECHNOLOGY

CROSSOVER

DOCTORAL DISSERTATIONS